ERROR IN HIGH–RESOLUTION SATELLITE RAINFALL PRODUCTS IN STREAMFLOW PREDICTION IN BIRR WATERSHED, ETHIOPIA

M. Sc. THESIS

NEBIYU SOLOMON

MAY 2013

ETHIOPIAN INSTITUTE OF WATER RESOURCE

ADDIS ABABA UNIVERSITY

Nebiyu Solomon Demisse

“BUILDING ETHIOPIA’S WATER FUTURE TOGETHER”

Addis Ababa University

P.O.Box 1176, Addis Ababa, Ethiopia
T +251-11-1239 768
F +251-11-1239 752
I www.aau.edu.et

Ethiopian Institute of Water Resources

P.O.Box 150461, Addis Ababa, Ethiopia
T +251-11-1223 344
F +251-11-1239 480
E info@eiwr.org
I www.eiwr.org

A M.Sc Dissertation on: Error in High–Resolution Satellite Rainfall Products in Streamflow Prediction in Birr Watershed, Ethiopia

Proposed By:

Nebiyu Solomon Demisse (B.Sc)
nebiyu.demisse@uconn.edu

Supervised By:

Dr. Mekonnen Gebremichael: from Uconn mekonnen@engr.uconn.ed

Dr. Menber Meles: from Uconn bitew@engr.uconn.ed

Submitted on:

May, 2013
Addis Ababa, Ethiopia.

Error in High–Resolution Satellite Rainfall Products in Streamflow Prediction in Birr Watershed, Ethiopia

A Thesis Submitted to the Ethiopian Institute of Water Resources Addis Ababa University in partial fulfillment of the requirements for the degree of Master of Science in Water Resource Engineering and Management (Surface Water Engineering and Management)

By

Nebiyu Solomon

May 2013

Addis Ababa University

STATEMENT OF AUTHOR

I declare that this thesis is my work and that all sources of materials used for this thesis have been duly acknowledged. Further I declare that when research paper is published from the thesis following sentence will appear at the bottom of the first page of the article or at the end of the article.

Name: _____ Signature: _____ Date:_____

Acknowledgements

I testify of God's mercy and grace that was sufficient for me throughout my studies at Ethiopian Institute of Water Resource (EIWR) Addis Ababa University.

I would also want to give special thanks to United States Agency for International Development (USAID) for sponsoring my studies under the USAID/HED funded grant in the Africa – US Higher Education Initiative - HED052-9740-ETH-11-01.

I would also want to extent my great appreciation and special thanks with all of my respect to my supervisors Dr. Mekonnen Gebremicheal and Dr. Menberu Melese for their constant support, excellent guidance, invaluable suggestions, and advice in every stage of my thesis. I greatly acknowledge Dr. Mekonnen for providing and facilitating field instruments. I thank Dr. Menberu for his quick response, for his assistance during rain gauge installation and providing satellite rainfall data.

Furthermore I would like to thank Prof. Jan Seibert for his quick replies, providing the HBV – light model setup and for his valuable support on input data preparation.

Finally I give special thanks to Dr. Tena, and all my lecturers, who helped me with great ideas throughout the beginning of the courses to the completion of the thesis. I am very thankful to Worku for his immediate response and facilitating the field trip during rain gauge installation. I am also grateful to my parents, brother, and friends for their prayer and support. Brook, Hewi, thanks so much for the motivation and other forms of support. Thank you all!!!

Table of Contents

List of figures

List of tables

Appendix I Tables

Appendix II Figures

Abstract

The main objective of this study is to evaluate the performance of high – resolution satellite rainfall products (TMPA 3B42RT, 3B42V6, and 3B42V7) under sparse ground based data and complex topography medium sized watershed (Birr at 952.8 km^2) in Blue Nile River basin Ethiopia through semi – distributed hydrological model HBV – light for daily streamflow simulation. First, the model is calibrated for the watershed to average rainfall input from rain gauge for the period of 2003 – 2008. Then the calibrated parameter values are used for daily streamflow simulations using rainfall input from each satellite products; comparison of the magnitude of rainfall and simulations to the observed streamflow at the outlet of each watershed forms the basis for the conclusions of this study. The comparison results of rainfall magnitudes revealed that both new version 7 TMPA 3B42RT and 3B42V7 rainfall estimates gave reasonably accurate result compared to rain gauge rainfall estimates. This result reveals that, in this region, 3B42RT accurately estimated the total average rainfall with negligible bias, but underestimated the seasonal rainfall with % bias less than -11 %; while very small overestimation of average seasonal and total rainfall observed in 3B42V7 rainfall estimates with % bias less than 6%. However; version 6 TMPA 3V42V6 rainfall estimates consistently underestimated both the total and seasonal rainfall with % bias greater than – 40%, which probably suggests that rainfall estimates based on TMPA 3B42V6 can't be a replacement of rain gauge measurements in this region. The result of this study revealed the applicability of satellite rainfall products as an input in hydrological model to simulate streamflow. Simulation from all rainfall inputs captured the trend of observed hydrograph with slight underestimation of large flood events. Simulation based on the new version 7 of TMPA 3B42RT and 3B42V7 gave reasonably accurate streamflow simulation for large flood events compared to others. On the other hand, the 3B42V6 simulation shows poor performance which underestimates consistently the daily streamflow. Dense rainfall network for rainfall measurement and stage – discharge rating curves should be given priority to improve the comparison results.

Key words: Satellite rainfall products, HBV – light model, Birr watershed.

CHPTER ONE

1. Introduction

1.1. Background

The growing availability of high resolution (and near real-time) satellite-based rainfall estimates has significant potential in applications such as hydrological analysis for engineering design, assimilation of precipitation information into forecast models, flood forecasting and water resources management in general. These applications would even have far – reaching effects for several developing countries whose ground based – rain gauges are sparse and no radar technology for measuring representative rainfall magnitude. However, there are errors associated to satellite based rainfall estimates which prompt several scientific questions. How accurate are satellite based rainfall products? Can high resolution satellite rainfall products be used for hydrological applications? Lack of knowledge on the accuracy of those satellite products is a challenge to the hydrological community especially under complex terrain and less gauged regions.

In this study, we investigate the Tropical Rainfall Measuring Mission (TRMM) Multisatellite Precipitation Analysis (TMPA) (Huffman et al. 2007) products over the complex terrain regions of Ethiopia in Birr watershed. TMPA products are developed by the National Aeronautic and Space Administration (NASA) Goddard Space Flight Center (GSFC). The high spatio – temporal resolution (~ 0.25^0 and 3 hourly) are available from 50^0 N to 50^0 S. In this study we evaluated three different TMPA products: TMPA 3B42RT (near real – time version), TMPA 3B42-V6 research version which is rain gauge based bias adjusted product and TMPA 3B42-V7 product which is newer version of rain gauge bias adjusted product. These products have made use of the possibilities to combine measurements of different space – borne sensors and gauge data which allows the derivation of high quality precipitation estimates. Huffman et al. (1995, 1997) created a scheme to combine satellite data of different sensors: Microwave (MW) accurate but infrequent, infrared (IR), frequent but less accurate with gauge data. The Tropical Rainfall Measuring Mission (TRMM) Multisatellite Precipitation Analysis (TMPA) the only space-borne sensor which includes radar measurements, method uses MW data to calibrate the IR-derived estimates and creates

estimates that contain MW-derived rainfall estimates when and where MW data are available and the calibrated IR estimates where MW data are not available.

Satellite rainfall products are subject to various source of errors related to temporal sampling, instrument, algorithm, gaps in revisit times, indirect relationship between remotely sensed signals and rainfall rate, (Gebremichael et al., 2005, Bitew and Gebremichael 2011) and also its performance varies with region, elevation, and season (Romilly and Gebremichael, 2011), therefore; it's very important to assess the performance and accuracy of these estimates. Previous works (Bitew et al., 2011 and Bitew and Gebremichael, 2011) found out that in complex terrain region of Ethiopia, the 3B42-V6 TMPA algorithms of merging satellite based estimates with range observation has magnified the error than improving the estimation accuracy. Many other studies have evaluated the performance of version 6 TMPA products with other high resolution satellite rainfall estimates like the TMPA 3B42RT (e.g. Su et al., 2008, Jiang et al., 2012,. Stesen and Sandholt., 2010). NASA revised its version 6 estimates and created version 7 products based on those studies. But there are only few studies on the evaluation of the version 7 products (e.g. Kirstetter et al., 2013, Chen et al. 2013).

A number of studies assessed the accuracy of satellite rainfall products on streamflow simulation capability using hydrological models. The satellite rainfall products performances are assessed with respect to the output of the hydrological model rather than with respect to the precipitation. Bitew and Gebremichael, (2011), for instance, compared the Climate Prediction Center morphing method (CMORPH), Precipitation Estimation from Remotely Sensed Information Using Neural Networks (PERSIANN) and the real-time version of the Tropical Rainfall Measuring Mission (TRMM) Multisatellite Precipitation Analysis (TMPA) 3B42RT) and TMPA 3B42 data with rain gauge data for two medium scaled watersheds of the Ethiopian highlands as input to hydrological model. This results revealed 3B42RT and CMORPH simulations show reliable skills in their simulations but underestimates large flood peaks, while 3B42 and PERSIANN simulations have inconsistent performance. Also this result showed the simulation based on satellite-only product (3B42RT) gave better performance than satellite-gauge product (3B42).

This study involves deployment of dense rain gauges over Birr watershed for high quality data collection over the summer period 2012, collection of historical rainfall data from existing rain

gauges and observed streamflow measurements and application of HBV hydrological model to simulate streamflow. The rainfall data sets and the modeling activities were used to characterize and determine uncertainty in input precipitation data; high resolution satellite rainfall estimates in this case. The overall study was conducted in three steps. These are 1) evaluation of the quality of daily rainfall measurements from existing rain gauges, data from newly deployed rain gauges over the summer period of 2012. 2) Evaluation and comparison of streamflow predictive skills using measurements from existing rain gauges and newly deployed rain gauges and 3) evaluation of uncertainty in satellite based rainfall estimates using satellite based simulated streamflow.

The main objective of this study is to evaluate the performance of high – resolution satellite rainfall products on prediction of streamflow using hydrological modeling under sparse ground based data and complex topography medium sized watershed in Blue Nile River basin of Ethiopia. Chapter 2 describes the literature review related to the objective of this study. First of all, rainfall measurement issues and high – resolution satellite rainfall products are discussed. Then we present the process that take place in a catchment which is necessary to understand streamflow modeling. Next, a description of hydrological cycle and rainfall – runoff processes are given and an overview of rainfall – runoff model is discussed. Chapter 3 provides a brief description of study area. The characteristics and location of Birr watershed, newly deployed rain gauges, existing rain gauges, and streamflow outlets. To achieve the objective of this study, the methods and data of the study will be discussed in chapter four. Then the interpolation technique used to generate areal rainfall and a description of HBV light model is presented. Model parameters and setup determination is described in this chapter. Furthermore, calibration of model is also discussed. Chapter 5 presents the comparison result of rainfall magnitude from existing and newly deployed rain gauges, and streamflow prediction from high – resolution satellite rainfall products. Finally, in chapter 6 the conclusion of this study is presented.

1.2. Objectives

1.2.1. General Objective

The main objective of this study is to evaluate the performance of high – resolution satellite rainfall products under sparse ground based data and complex topography medium sized watershed. The study makes use of information acquired from newly deployed sensors, historical hydro-climatic data from existing observation and a semi – distributed hydrological modeling system.

1.2.2. Specific Objectives

To attain the above main objective the following specific objectives are derived.

- To compare satellite rainfall products with ground based rain gauge rainfall both averaged over the watershed.
- To calibrate the HBV – light model using ground based hydrological and meteorological data over the watershed at daily time step.
- To evaluate streamflow simulation capability of high resolution satellite rainfall products over the watershed.

1.3. Research questions

This study will address the following inter-related research questions.

- Can high – resolution satellite rainfall products accurately estimate rainfall compared to ground based rain gauge rainfall observation over Birr watershed?
- Can measurements from sparse rain gauges represent arael rainfall estimates of Jiga watershed? Can they be used to evaluate the accuracy of high – resolution satellite rainfall products?

- How good area high – resolution satellite rainfall products for prediction of streamflow?

CHAPTER TWO

2. Literature Review

2.1. Introduction

This chapter describes the literature review related to the objective of this study. Among various component of the water budget, rainfall is the primary driver of global atmospheric circulation as a hot source, it is necessary to quantify this rainfall component in hydrological cycle. Therefore; first we describe rainfall measurement technique and satellite rainfall products. Then understanding spatial distribution of rainfall to compute average areal rainfall is also very important in rainfall – runoff modeling, since most of the time the output of models is subject input uncertainty. Next, a description of hydrological cycle and rainfall – runoff processes are given and an overview of rainfall – runoff models is also discussed. Moreover, application of high – resolution satellite rainfall products in hydrological modeling was presented.

2.2. Rainfall Measurement

Precipitation is one of the main components in the hydrological cycle and knowledge of rainfall and its variability is therefore crucial to understand and to predict the global climate system. Also rainfall data with very fine resolution and high quality are of primary importance for hydrological computations (Clemens and Bumke, 2001). Haile et al., (2009); hydrological model output is highly affected by rainfall input uncertainty. In spite of its important role in our lives and global climate, the measurement of rainfall is extremely difficult because of its high spatial and temporal variability's. Dense rain gauge network provides the most reliable rainfall data measurements, but it only gives a point rainfall data. In practice, the density and configuration of a rain gauge network is determined based on the availability of funds, accessibility of site and the purpose of the network. As a result most of the time rain gauges in developing countries are commonly installed in towns that are located along main roads that provide accessibility. However, relatively remote and mountainous areas may remain uncovered by the rain gauge network. Satellite remote sensing is probably the way to provide rainfall data on a global scale.

2.3. Description of satellite rainfall products

The Tropical Rainfall Measuring Mission (TRMM) space-borne rainfall sensors are becoming an object of interest by the scientific community. The design of this sensor follows the development of algorithms to estimate the 3D rain distribution from visual spectrum radiance, radar and microwave sensors (Zhong et al. 2002).

The great advantage of space-based precipitation estimates is their global coverage, providing information on rainfall frequency and intensity in regions that are inaccessible to other observing systems like rain gauge and radar. The disadvantage is that they are indirect estimates of rainfall, depending on the properties of cloud top (in the case of IR algorithms) and cloud liquid and ice content (in the case of passive microwave algorithms). Active radar observation from the TRMM Precipitation Radar provide the most accurate high resolution satellite based rainfall estimates to a date, but the sampling characteristics of this instrument are quite limited (Ebet, 2007).

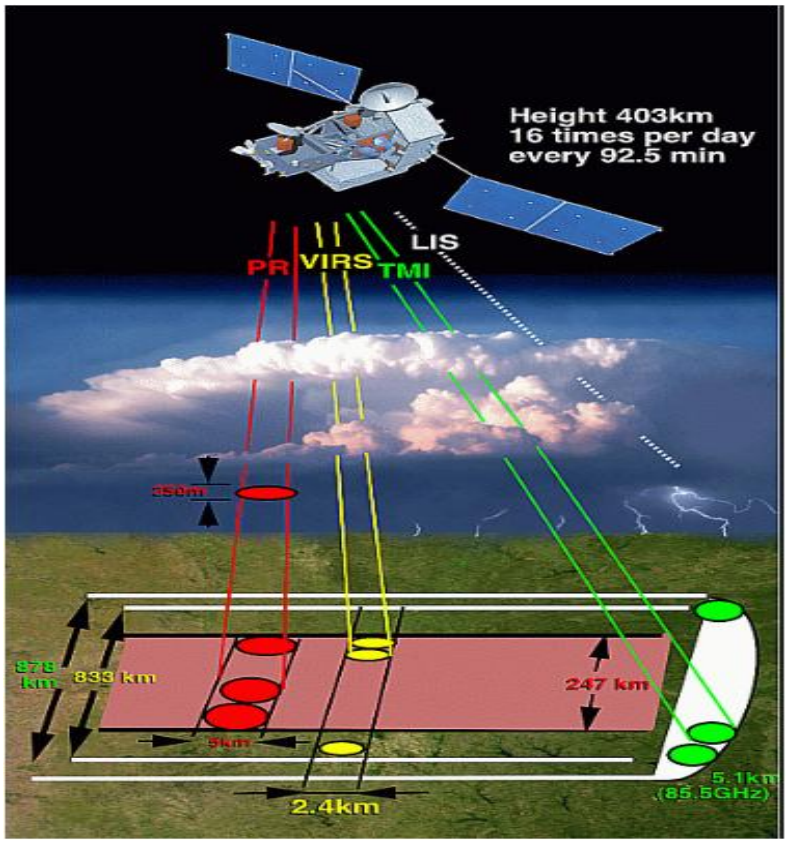

Fig.2.1. TRMM satellite and instruments

The work of Tropical Rainfall Measuring Mission was an international project which carried out by, the National Aeronautics and Space Administration (NASA) of USA and the Japanese Aerospace Exploration Agency (JAXA), designed to provide improved precipitation estimates in the Tropics, where the bulk of the Earth's precipitation occurs. NASA and JAXA launched TRMM satellite on November 27, 1997 and TRMM began recording data in December 1997.

TRMM travels in a non-sun-synchronous 403 km height orbit at 35^0 inclination angle. The spacecraft takes about 91 minutes to complete one orbit around the earth. This orbit allows as much coverage of the tropics and extraction of rainfall data over the 24 hour day (16 orbits) as possible. The revisit time for the TRMM satellite is around 15 hours (NASA/GSFC, 2007).

The TRMM observatory includes five science instruments[1] – figure 2.1 and table 2.1 namely: the Precipitation Radar (PR), the TRMM Microwave Imager (TMI), the Visible and Infrared Scanner (VIRS), the Clouds and the Earth's Radiant Energy System (CERES), and the Lightning Imaging Sensor (LIS). TRMM has three instruments (PR, TMI, and VlRS) in its rainfall measurement package, to obtain tropical and subtropical rainfall measurements, rain profiles, and brightness temperature.
TRMM has the only passive microwave instrument (TMI) in an inclined orbit and the first and the only rain radar in space. The three rain instruments are providing the most complete rain data set (to date) in order to generate climate models and perform severe storm studies.

The two additional instruments flown on-board TRMM are the CERES and LIS. CERES and LIS are flown on board TRMM as instruments of opportunity for the Earth Observation System Program. The CERES instrument measures the Earth's radiation budget, and the LIS instrument investigates the global distribution of lightning.

It is believed that the TRMM satellite provides more accurate observation measures spatio-temporal coverage and intensities of precipitation over the tropics (Shin et al. 2001). To improve the TRMM data quality, TRMM products are constantly reprocessed, as new information acquired by TRMM lead to improved algorithms.

---

[1]TRMM Instruments: *http://disc.gsfc.nasa.gov/precipitation/instrument trmm.shtml*

Table 2.1. TRMM precipitation-related instruments.

Instrument name	Band frequencies/ wavelength	Spatial resolution (km)		Swath width (km)	
		Pre-boost	Post-boost	Pre-boost	Post-boost
Visible and Infrared Scanner (VIRS)	5 channels (0.63, 1.6, 3.75, 10.8, and 12 μm)	2.2	2.4	720	833
TRMM Microwave Imagery (TMI)	5 frequencies (10.7, 19.4, 21.3, 37, 85.5 GHz)	4.4 (at 85.5 GHz)	5.1 (at 85.5 GHz)	760	878
Precipitation Radar (PR)	13.8 GHz	4.3 (Vertical 250 m)	5 (Vertical 250 m)	215	247
Lightening Imaging Sensor (LIS)	0.7774 μm	3.7	4.3	580	668

Recently, the TRMM reprocessing was completed using version 7 algorithms- Figure 2.2. To achieve the best possible results, TRMM has developed many algorithms and the most recently ones are the TRMM Multisatellite Precipitation Analysis (TMPA) method post-real-time research version 7 products 3B42V7.

2.3.1. Algorithms of TRMM Multisatellite Precipitation Analysis

The purpose of algorithms TMPA 3B42 and 3B42RT, Figure 2.3 is to produce TRMM rainfall retrievals merged high quality (HQ)/ infrared (IR) precipitation and root mean square (RMS) precipitation error estimates. The data include retrievals from six different algorithms: VIRS, TMI, PR, and the combination with other satellites (GPI, GPCP and SSMM). Table 2.2 provides the definition of the TRMM products at each level

Table 2.2: The definition of the TRMM products

Level	Definition
0	Unprocessed instrument data, time ordered, qulity checked, no redundancy.
1	Ancillary data and georeferencing data attached to Level 0, and processed to sendor-dependent physical units (e.g. radar reflectivety, brightness, temperature)
2	Meteorological parameters (e.g. rainfall rate) derived from Level 1 data using various algorithms, which will be provided as a 2-or3-dimensional rain map along the TRMM swath.
3	Results of mapping the meteorological parameters (Level 2) on a uniform space and time grid.

The 3B42 is composed of two separate algorithms, which are (i) to produce monthly IR calibration parameters, and (ii) to calibrate the merged-IR precipitation data to produce the daily adjusted merged-IR precipitation and RMS precipitation error estimates (JAXA, 2006).

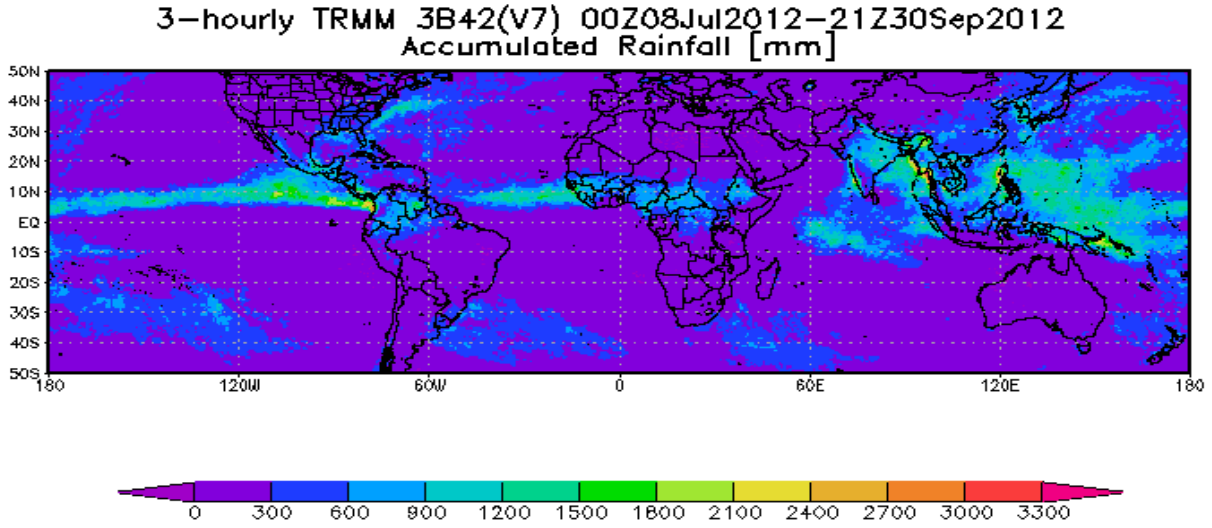

Fig. 2.2 Three-hour TRMM 3B42 (V7) 08, July - 30, Sep, 2012, accumulated rainfall [mm]

---

[2]3-hour TMPA-RT accumulated rainfall [mm]:

http://disc2.nascom.nasa.gov/Giovanni/tovas/realtime.3B42RT.2.shtm1

2.3.2. Data set

The TRMM Science Data and Information System (TSDIS) operate under the Global Change Data Center at GSFC. Its primary function is to process rainfall instrument science data from the TRMM spacecraft, and distribute the products to TRMM science algorithm developers, scientists performing data quality control (JAXA, 2006).

The Goddard DAAC maintains archive of all TRMM data products. The data is provided as Hierarchical Data Format (HDF) that is the native format for TRMM data. Another way to acquire the files can be ordered via FTP network (GES DISC, 2006).

Recently, TRMM Online Visualization and Analysis System (TOVAS) provide files into formats readily importable into the GIS, it takes the .HDF file and generates any of the following formats: *.txt, *.csv, and *.asc for all or a subset of the source file (GES DISC, 2006).

2.4. Streamflow analysis

Catchment response to the event is characterized by measuring the discharge (volume rate of flow) at the outlet. This is described by a hydrograph. It is clear that hydrograph is a spatial and temporally integrated response of catchments which is determined by spatially and temporal variation of input (rainfall), and travel time of each drop of water form where it strikes on the stream network to outlet. After begins of the rainfall event the flow rate to basin increases rapidly and at same moment it reaches the peak discharge. Each hydrograph has a different shape because it depends on the catchment input (rainfall), and the catchment characteristics. Knowledge of climatic factors (precipitation, evaporation, and transpiration), geometric factors (size, shape, elevation, and stream density), geology, soil type, and landuse as well as channel factors (size, shape of the channel, cross-section, slope, length, roughness, and number of tributaries) is very important. Catchment response to an event is characterized by the discharge (volume flow rate) at the outlet that is described by a hydrograph. Sometime after the start of the event the flow rate begins to increase till the well defined peak discharge. At this moment the hydrograph rises, which characterized by the rising limb. After that the hydrograph declines as a result of ending of direct runoff, which is described by the recession limb. At the recession period, the discharge is related primarily to the base flow. From this description, one can identify the hydrograph

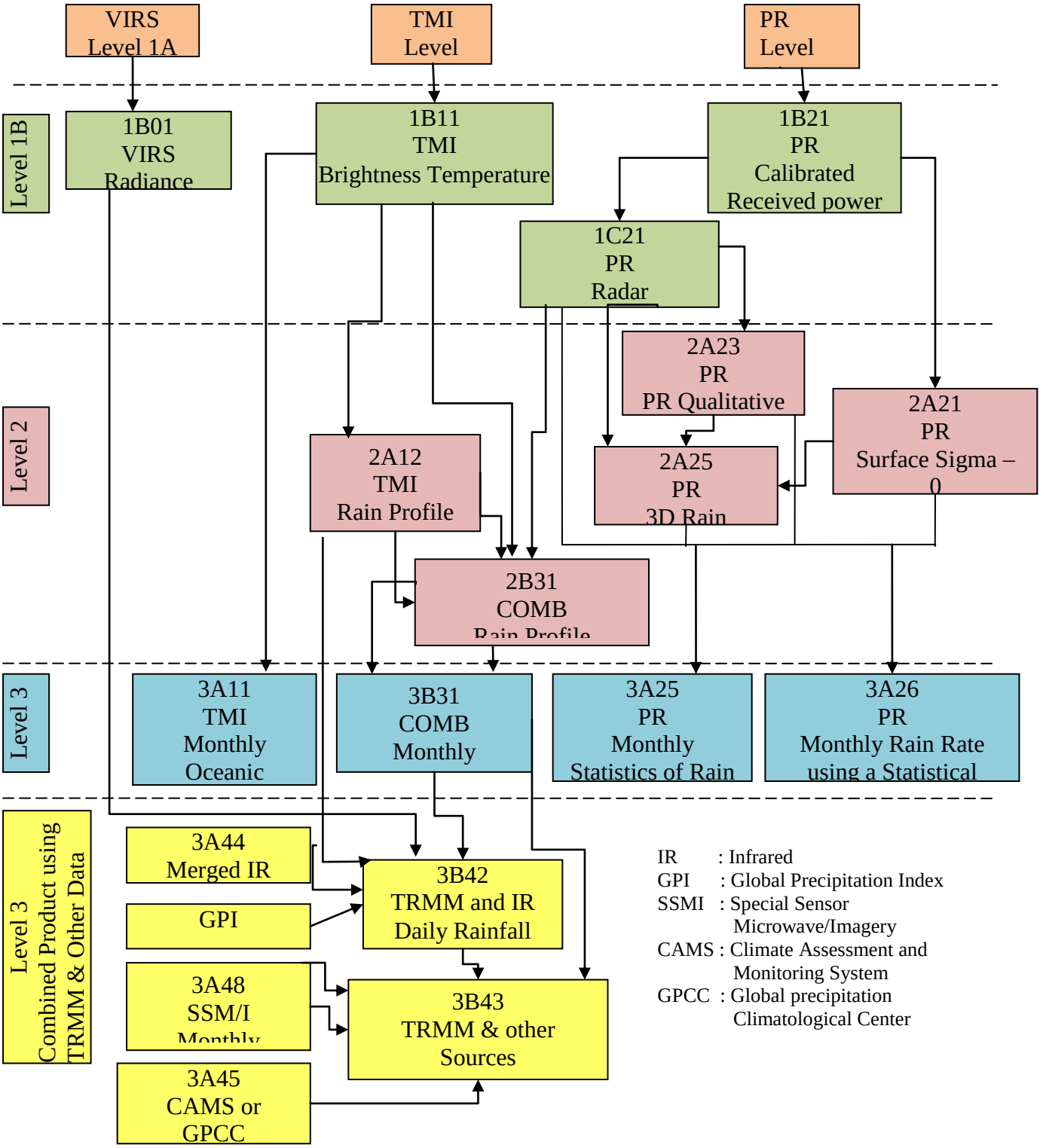

Fig.2.3. TRMM Algorithm Flow Diagram

components that are overland flow, interflow, and base flow. Here, the streamflow recession analysis is used based on the work of Linsley et al. (1958)

2.5. Hydrological cycle and rainfall – runoff processes in a catchment

The most important processes related to hydrological cycle are presented Figure 2.4. Precipitation is a primary factor in hydrology and is the main input of water to land surface. Knowledge of the spatial and temporal distribution of rainfall in hydrological modeling is very important. Rainfall partly intercepted by the vegetation canopy before it reaches the ground surface. The quantity of rain captured by trees, plants, depends not only on their sort, stage of development, and density of vegetation canopy, but also on the intensity and duration of precipitation. For rainfall – runoff, interception is considered as a loss.

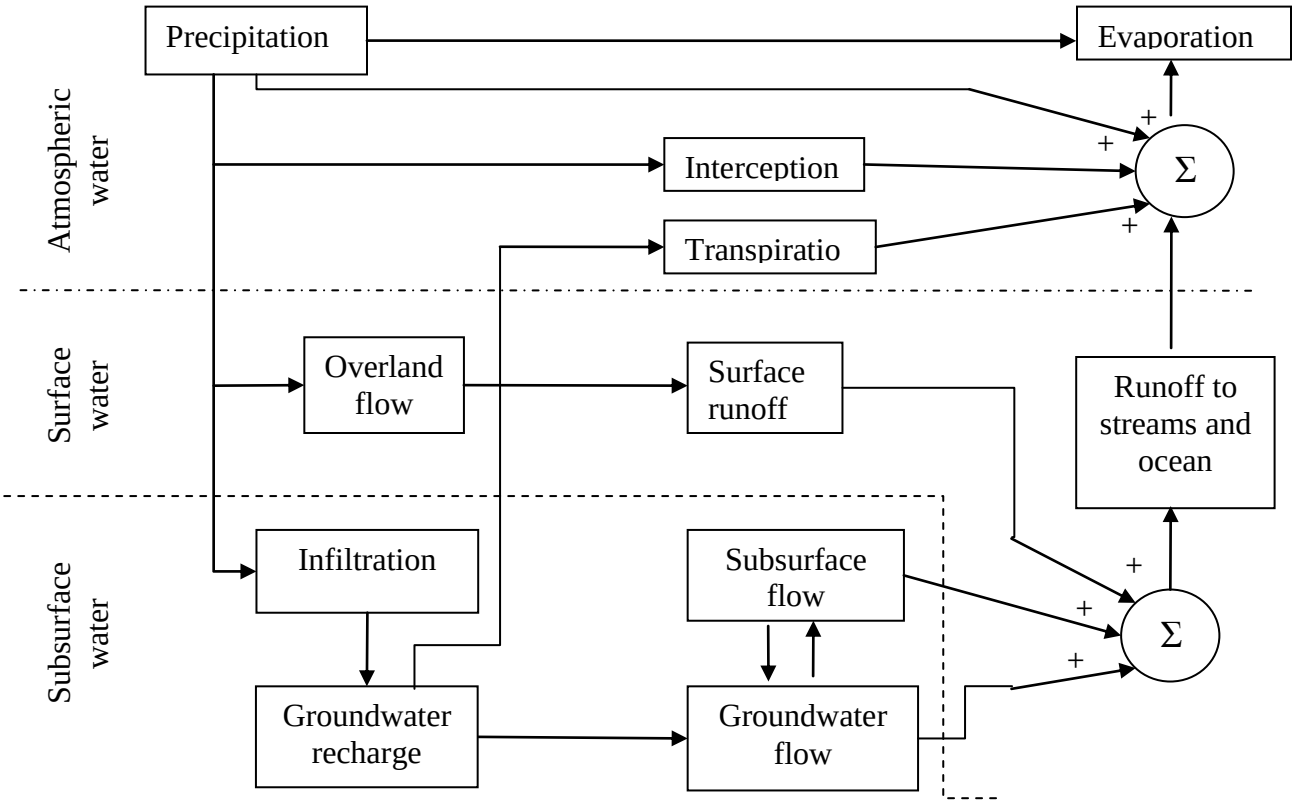

Fig. 2.4 Hydrological cycle

The remaining rain that reaches the ground either evaporates, infiltrates, or remains at the land surface as overland flow. Infiltrated rainfall may percolate to recharge the saturated domain, but also may flow to a channel through interflow. Due to evaporation and transpiration at the land surface the water availability in the subsurface reduces. On the other hand, due to an intensive rainfall event groundwater level may rise and water starts to move from saturated zone toward

unsaturated zones as capillary rise. The dominant flow processes that contributes to catchment are difficult to understand because hydrological domains (overland, unsaturated, saturated and channel) are coupled. In reality several flow processes can be distinguished, Horton overland flow, this occurs when the intensity of the rainfall is greater than the infiltration capacity of the soil. Due to this water is stored at the land surface. According to (Dunne 1983) Horton overland flow is common in arid and semiarid zones when rainfall events are very intensive and the vegetation cover is poor. When the soil is saturated due to rise of groundwater level to the land surface the saturation overland flow is generated. Saturated overland flow is typical for humid zones. Finally, channel flow occurs when the water reaches the catchment drainage system.

Flow processes do not occur only at the land surface, but also occurs in the subsurface. Indeed, due to infiltration water enters the subsurface as unsaturated flow in the form of matrix or macro pore flow. When the saturated hydraulic conductivity of a given layer is lower compared to the layer above, perched subsurface flow is generated. In the saturated zone groundwater flow can be rapid or delayed. Groundwater flow is very important component for the base flow.

2.6. Rainfall – Runoff modeling

Understanding the rainfall – runoff relation has been a subject of hydrological research for a long time (Ragan 1968, Betson and Marius 1969). These studies have concluded that runoff occurs due to a complex interaction between surface, unsaturated, and saturated flow. In the same time researches in the field of hydrology focused on streamflow simulation processes using hydrological model. A model is a representation of the real world into a conceptual world. It is obvious that modeling the flow processes that occur in the real world will be simplified in modeling. However, these models should be able to capture the dominant processes at different space and time scale in a catchment. Models can be predictive (to obtain a specific answer to a specific question) or investigative (to further understanding hydrological processes) (O'Connell 1991). Another classification of hydrological models is given in the report of World Meteorological Organization (WMO, 1990), which divides the models in two classes: deterministic model (models, which value of all parameters are uniquely defined) and stochastic models (models having probability distribution in parameter space). N. Engida et al. (2011) used Modified Bartlett – Lewis Rectangular Pulse Model (MBLRPM), which is a stochastic point – process disaggregation rainfall model, to characterize and disaggregate daily rainfall in the Upper Blue Nile Basin, according to

study, disaggregation of daily rainfall was poor compared to observed hourly rainfalls. However the result was improved when outputs of the (MBLRPM) redistributed using relevant probability distributions to simulate the diurnal rainfall pattern. Within the deterministic model, which is focus of this study, three types of modes are distinguished based on spatial discretization. In rainfall – runoff modeling, models are characterized as lumped, semi-distributed, or distributed. Lumped models deal with a catchment as a single unit, which means that the heterogeneities are ignored and the input data are averaged. S. Uhlenbrook et al. (2010) conducted catchment modeling to understand water balance dynamics and runoff generation mechanisms in 5000 km^2 catchment in Ethiopia using lumped, lumped with multiple vegetation zones, and semi – distributed with multiple vegetation and elevation zones. According to this result, model result was not satisfactory due to limited data quality and model insufficiencies, and concluded that detailed hydrological processes are not captured in an ungauged area. On the other hand, distributed models considers for spatial variability of topography, geology, soil type, and landuse/cover within a catchment. D. Legesse et al. (2003) analyzed hydrological response of a catchment to climate and land use changes using the physically based distributed Precipitation Runoff Modeling System (PRMS) (Leavesley et al., 1983, 2002) in Ketar river catchment within the Ziway–Shala basin, South Central Ethiopia, this study revealed "Based on sensitivity analyses, a 10% decrease in rainfall produced a 30% reduction on the simulated hydrologic response of the catchment, while a 1.5 8C increase in air temperature would result in a decrease in the simulated discharge of about 15%. Converting the present day dominantly cultivated/grazing land in the studied river basin by woodland would decrease the discharge at the outlet by about 8%. Rainfall measurement and stage-discharge rating curves should be given priority to improve model performance". Based on the objective of this study Hydrologiska Byråns Vattenbalansavdelning (HBV-light) model applied at daily time step to assess the performance of high resolution satellite rainfall products.

2.7. Application of high – resolution satellite rainfall products in hydrological modeling

A number of studies have been carried out to assess the capability of satellite rainfall products through streamflow simulation using hydrological modeling. We summarized some of the studies that evaluated the performance of satellite rainfall products for hydrological simulation as follow: These studies revealed the capability of satellite rainfall products in the application of hydrological modeling.

Table 2.3. Studies on performance of satellite rainfall products through hydrological modeling.

Satellite rainfall products evaluated	Hydrological model used	Watershed characteristics	Main results	References
CMORPH, TMPA 3B42RT, TMPA 3B42 and PERSIANN)	SWAT (Arnold et al. 1998)	Gilgel Abay at 1656 km^2 Koga at 299 km^2, Ethiopian highlands.	TMPA 3B42RT and CMORHP – based model simulations were performed better compared to TMPA 3B42 and PERSIANN. Also simulation based on 3B42RT and CMORHP improved when watershed area increases while 3B42 and PERSIANN based deteriorates.	M. Bitew and M. Gebremichael, (2011).
Satellite-based rainfall estimates (SBRE) (Xie and Arkin 1997)	Geospatial Stream Flow Model (GeoSFM) (Artan et al. 2001)	2646 km^2, Nyando Kenya 6044 km^2, Se Done, China 19013 km^2, nam Ou, China 22150 km^2, Gash, Ethiopia – Eritrea – Sudan	SBRE – based model simulation performed better when model was calibrated with satellite data than with sparse rain gauge data.	Artan et al. (2009)
TMPA 3B42 (Huffman et al. 2007)	SWAT (Arnold et al. 1998)	7720 km^2, middle Nueces, Texas 8950 km^2, midlle Rio Grande, Mexico – united States	While simulation with ground – based radar data were superior, TMPA 3B42 – based data were acceptable and comparable to those based on rain gauge data.	Tobin and Bennett (2009)
CMORPH, TRMM3B42 and PERSIANN)	Hillslope River Routing (HRR) model (Beighley et al. (2009)	3.7 Million km^2 Congo Basin, the world's second largest river basin.	The three satellite product vary significantly in terms of magnitude but produces a reasonable streamflow hydrograph, overall this study revealed that, TRMM (3B42) performed best in spatial and temporal distributions and magnitudes while CMORHP and PERSIANN tend to overestimate.	R.E.Beighley et al. (2011)

CHAPTER THREE

3. Description of study area

3.1. Location on study area

The Birr watershed (952.8 km^2) is one of the tributary river basins of upper Blue Nile Basin which is located in the North – Western Ethiopian highlands. It is located in the middle of the Blue Nile River basin within 10.5^0 – 11.25^0 N and 37.25^0 – 37.75^0 E. Within or around the watershed, there are around, four existing rain gauges (non-recording), eleven newly installed Tipping Bucket (Hobo-S-RGA-M002) rain gauges (recording), which is installed in June 2012 for this study, and one outlet at the lowest point of the watershed (Figure 3.1). The watershed was characterized by complex terrain with elevation ranging from 1771 m to 3257 m a.s. l.

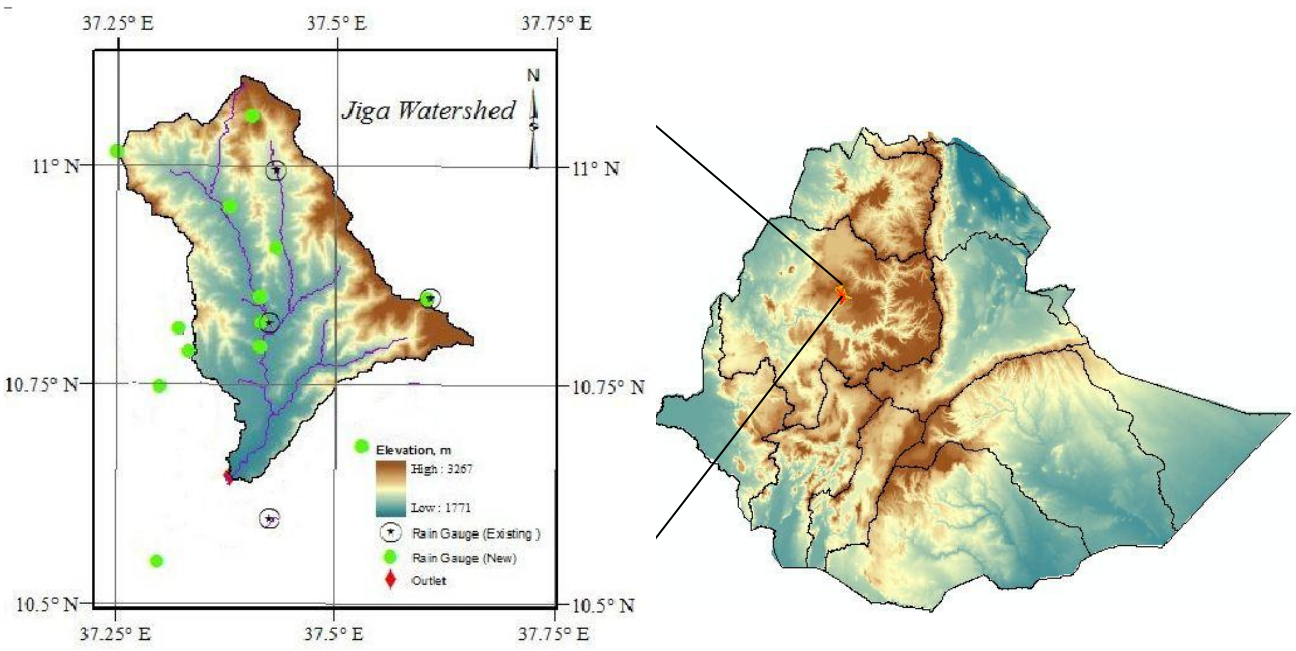

Fig.3.1 Birr watershed map (left). Location of Birr watershed within the map of Ethiopia in Blue Nile River basin (right). Birr watershed map showing its watershed and subwatershed boundaries, elevation, river network, location of new rain gauge, existing rain gauge and stream flow gauge stations.

3.1.1. Climate

A complex topography of the Birr watershed has a strong influence on meteorological phenomena in the region. The mean annual rainfall recorded at different stations is 1342 mm with only one rainy season (mono-modal) which lasts from the June to end of September and the mean maximum and minimum temperature were 29.6 ^{0}C and 14 ^{0}C respectively. This watershed is part of intertropical convergence zone.

3.1.2. Topography and geology

Birr watershed is dominated by high elevation, which ranges from 1771 – 3257 meter above sea level. The upstream part is characterized by a mountain area with very steep slope while downstream part is flat area. Volcanic rocks predominantly cover the study area. These rocks exhibit greater variation in their water bearing properties. The aquifers of the study area in relation to potential production are not evaluated significantly. This may be due to the fact that there is no any borehole, hand dug wells and springs are insufficient and unevenly distributed to make quantitative evaluation of the aquifer system. In spite of all these limitations, existing geologic, geomorphic and structural information, and some spring hand dug well discharges provides some highlight about the ground water condition of the area and the nature of the aquifer with certain degree of certainty.

3.1.3. Soil

The soil of Birr watershed is classified as Luvisols, Vertisols, Cambisols, and Nitosols following the classification of FAO-Unesco (1990). The Luvisols dominates the watershed while cambisols are present in small portion in the catchment. In general, these types of soils are deep and fertile at gentle slope. The FAO-Unesco classification can be transformed into soil texture, which is important in hydrology. Luvisols are red soils mainly formed on nearly level to gentle sloping topography (0-5 %). These soils are best suited for agricultural production due to their good physical properties. These soils have good water holding capacity with no water logging problems making them suitable for major crops that are not restricted by the relatively colder weather conditions. The texture of vertisols and camisols are clay and sandy loam, respectively. Clay soils have high overland flow potential and very low maximum infiltration capacity. The landuse is dominated mainly by intensive cultivated (agriculture), grassland and state farm.

CHAPTER FOUR

4. Methods and data

4.1. Methods

To achieve the objective of this study, we evaluated the quality of daily average rainfall measurements from existing historical rain gauges, data from newly deployed rain gauges over the summer period of 2012. We also analyzed rainfall input uncertainty through streamflow predictive skills using rainfall from existing rain gauges (sparse) and newly deployed rain gauges (relatively dense) for the summer period of 2012. Then uncertainty in satellite based rainfall estimates using satellite based simulated streamflow were evaluated. Watershed averaged rainfall, temperature, evaporation, and observed streamflow data were used as an input in hydrological model.

4.1.1. Areal (average) rainfall computation

The areal rainfall computed is used as rainfall inputs to HBV – light hydrological model. The highly convective nature of rainfall in the study area restricts the use of interpolation methods such as kriging since it is difficult to construct the semi-variograms for convective events at daily time interval. As such, the areal rainfall at daily time steps was interpolated using the Thiessen polygon method which is also applied by Bergstr¨om, (1995) In general, the number of precipitation stations should be as high as possible to generate realistic interpolation pattern.

Based on the data available from three rain gauge stations here, the Thiessen polygon method for rainfall interpolation in Birr watershed was used.

$$\overline{P_j} = \sum_{i=1}^{N} C_i P_{ij} \qquad [4.0]$$

Where: $\overline{P}$ is the areal rainfall estimates, C_i is the Thiessen weight for station *i*, P is the rainfall depth recorded at a specific station, j is a time index, and N is the total number of rain gauge stations.

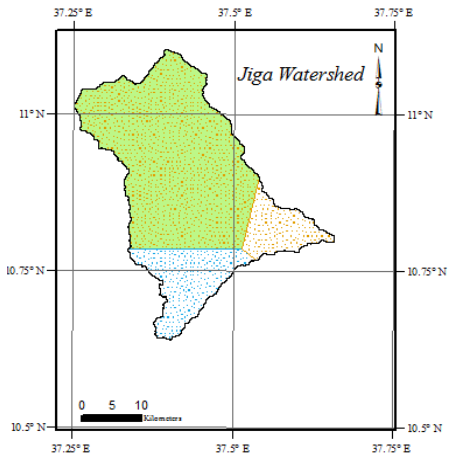

Fig. 4.1 Daily rainfalls from three rain gauge stations interpolated map of Birr watershed using Thiessen Polygon method.

4.2. Data

4.2.1. Newly deployed rain gauges

The rainfall data obtained from the network consisting of newly deployed eleven rain gauges (recording) in the valley and mountain area of the Birr watershed as shown in Figure 3.1. The rain gauges have a funnel diameter of 15.4 cm, a Tipping Bucket (Hobo-S-RGA-M002) mechanism with a resolution of 0.25 mm, and measurement range of 0 – 5 cm h^{-1}.

Fig. 4.2 A photographic view of Tipping Bucket rain gauge electronic recorder during its installation and data collection.

The rainfall collected from these rain gauges has fifteen minute temporal resolution and 6 km or less spatial resolution for the period of 08 July to 30 September 2012. To our understanding, the rainfall has never been monitored at high temporal and spatial resolution. Table 1 shows the characteristics of new rain gauge stations. Also, rainfall from all this station was used as input for hydrological models.

4.2.2. Existing historical rain gauges

This existing rain gauge stations were relatively sparse and have one day temporal resolution monitored by National Meteorological Agency of Ethiopia (NMAE). Existing rain gauges station consists of three rain gauges. We collected rainfall data from these three stations for the period of 2003 to 2008 from NMAE. Table 4.1 shows the characteristics of existing rain gauge stations.

4.2.3. Satellite rainfall products

In this study three high resolution satellite – based rainfall estimations (SREs) are evaluated, which estimates precipitation at the same spatial (0.25^0 by 0.25^0) and temporal (3-hourl) resolution. The SREs considered are (i) the Tropical Rainfall Measuring Mission (TRMM) Multisatellite Precipitation Analysis (TMPA) near-real-time product (3B42RT), (ii) the TMPA method post-real-time research version 6 & 7 product (3B42 V6 & 3B42 V7).

4.2.4. TMPA 3B42B V6, 3B42 V7 and 3B42RT satellite rainfall Products

The Tropical Rainfall Measuring Mission (TRMM) Multisatellite Precipitation Analysis (TMPA) near-real-time product (3B42RT), the TMPA method post-real-time research version product (3B42), have a global coverage between 50^0 N and S since 1998 (spatially completed since February 2000). The data is provided in 3 – hourly intervals on a $0.25^0 \times 0.25^0$ latitude – longitude grid. It is produced at the NASA Goddard Space Flight Center (GSFC) using TMPA. This method combines precipitation estimates of four passive microwave (PMW) sensors, namely TRMM Microwave Imager (TMI), Special Sensor Microwave/Imager (SSM/I), Advanced Microwave Scanning Radiometer-EOS (AMSR-E) and Advanced Microwave Sounding Unit-B (AMSU-B). These PMW sensors fly on a variety of satellite platforms, namely the TRMM, the Defense Meteorological Satellite Program (DMSP), the Aqua mission and National Oceanic and Atmospheric Administration (NOAA) satellites. They are calibrated with the TRMM Precipitation

Table 4.1 Characteristics and the location of newly installed new and existing rain gauge stations. Note that the coordinate system projection is GCS_WGS_1984 datum D_WGS_1984, Clark ellipsoid (1880).

	Geographic coordinate system (Degree decimal)			
Stations	Latitude	Longitude	Elevation (m)	Aspect
1. Newly deployed Rain gauges				
Atiha	10.7930	37.4144	1924	North East
Gentabo	10.8209	37.4262	1936	North East
Maksegnien	10.8147	37.3213	2184	North
Amstegna	10.7881	37.3317	2094	North
Dangber	10.7470	37.2996	2067	North West
Bahta	10.9060	37.4326	2047	North
Senebo	10.8498	37.4153	1985	North
Zanbit	11.0565	37.4041	2788	North East
Anjine	10.6792	37.5304	2417	South West
Feresbet	10.8485	37.6048	3001	South West
Lebagedel	10.9532	37.38	2027	West
Existing rain gauges				
Quarit	10.9959	37.4310	2147	East
Feresbet	10.8499	37.6084	3000	South West
Yechereka	10.5975	37.4249	2000	South

Radar (PR) – TMI combined instrument product to a high quality (HQ) microwave product. Where HQ microwave data for a certain location and time step is lacking, HQ-calibrated infrared (IR) data, referred to as "variable rain rate" (VAR), is used to fill the gap. The input IR dataset is produced by the Climate Prediction Center (NOAA/CPC; except a Global Precipitation Climatology Project, GPCP, product is used prior to 2000). The 3B42 product is composed of calibrated HQ microwave and VAR infrared data in 3-hourly, $0.25^0 \times 0.25^0$ resolution. The near-real time version, TRMM

3B42 RT (satellite only product), is produced approximately 9 - hours after observation time. The TRMM 3B42 is calibrated and merged with ground station data in the monthly resolution and subsequently rescaled to the final 3-hourly intervals (Huffman et al., 2007). The calibrating gauge analysis datasets are processed and provided until March 2005 by the Global Precipitation Climatology Centre (GPCC; GPCP global monthly rain gauge analysis; 1^0, monthly). The TMPA data can be freely downloaded at: http://mirador.gsfc.nasa.gov/collections/TRMM 3B42 006.shtml.

It should be noted that TRMM's orbital altitude shifted in August 2001 from 350 to 403 km. More importantly, the available constellation of microwave satellites has varied significantly over time (Huffman et al., 2007).

4.2.5. The transition from version 6 to version 7 for TRMM 3B42 data set

The transition from Version 6 to Version 7 for TRMM datasets occurred on 30 June 2011 for 3B42. Thereafter, the Precipitation Processing System (PPS) was reconfigured to start the parallel activities of Version 7 3B42 "initial processing" (IP) for new data (starting 1 July 2011 for 3B42), and Version 7 3B42 reprocessing (RP) for the entire archive starting 1 January 1998. The TMPA lagged the other TRMM products to allow for calibration and to finalize use of SSMIS data.

The new release version 7 incorporated several important changes: additional satellites, a new IR brightness temperature dataset for the period before the start of the CPC 4-km Merged Global IR Dataset (i.e., January 1998 – February 2000), uniformly reprocessed input data using current algorithms, use of a single, uniformly processed surface precipitation gauge analysis using current algorithms as computed by the Global Precipitation Climatology Centre (GPCC), use of a latitude-band calibration scheme for all satellites, and additional output fields in the data files, and including sensor-specific source and overpass time.

4.2.6. Streamflow data

In rainfall – runoff modeling, the streamflow data was used for calibration of the results obtained from model simulation. In this study, we also used two types of streamflow data (i) average daily streamflow data from hourly collected stream gage for rain period (July 8 to September 300 2012), which was collected for this study and (ii) daily streamflow data for the period of 2003 – 2008, which was relatively long period. All stream flow data were provided by Ethiopian Ministry of

Water and Energy (EMoWE). The Birr watershed stream gage located at 37^0 23' E and 10^0 39' N. Figure 4.3 shows the monthly observed streamflow and average rainfall from existing station.

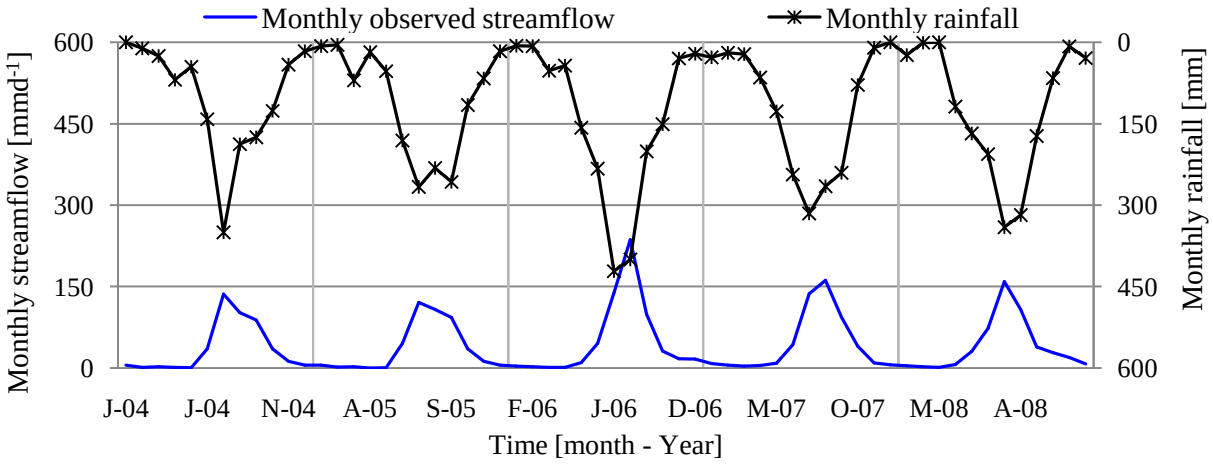

Fig. 4.3 Comparison of monthly observed streamflow and average rainfall data for the period of 2004 – 2008 over the watershed.

Daily evapotranspiration data collected from one research center located in the watershed for the period of 2003/2008.

4.3. Description of Hydrological model

A description of hydrological model is presented. Furthermore, to run these models it is necessary to determine the model parameters and to setup the model. We used a semi – distributed HBV – light model which is conceptual rainfall – runoff model for continuous calculation of runoff. It was developed by Swedish Meteorological and Hydrological Institute (SMHI) (Bergström, 1995; Lindstrom et al. 1997). The model uses subbasins as primary hydrological units and within these an area – elevation distribution and a classification of land use (forest, open and lakes) can be made. The new version of the model used in this study, HBV light (Seibert, 1996) corresponds to the version described by Bergstrom (1992) which has only two slight changes. HBV-light uses a warm-up period during which state variables evolve from standard initial values to their appropriate values according to meteorological conditions and parameter values; and in the original version, only integer values are allowed for the routing parameter MAXBAS. This limitation has been removed in the new version. In order to keep the program as simple as possible, several functions

found in the HBV-6 software were not implemented in the HBV light software. It is possible to use a correction of the long-term mean of potential evaporation values as proposed by Lindström and Bergström (1992). The HBV-light version provides two options which do not exist in the HBV-6 version. The first one is the possibility to include observed groundwater levels into the analysis and the second is the possibility to use a different response routine with a delay parameter.

The new model consists of different routines and simulates catchment discharge, on any time step, based on time series of precipitation and air temperature as well as estimates of monthly long-term potential evaporation rates. In the snow routine snow accumulation and snowmelt are computed by a degree-day method. In the soil routine groundwater recharge and actual evaporation are simulated as functions of actual water storage. In the response (or groundwater) routine, runoff is computed as a function of water storage. Finally, in the routing routine a triangular weighting function is used to simulate the routing of the runoff to the catchment outlet. The schematic model structure is given in the figure 4.4 below; more detailed descriptions of the model can be found elsewhere (Bergstr¨om, 1995; Lindstr ¨om et al., 1997; Seibert, 1999).

4.3.1. Model setup

In this study, a semi-distributed version of HBV – light model based on data availability and the characteristics of the Birr watershed was used. The watershed was divided into different range of vegetation, landuse and elevation zones. Precipitation, air temperature, and potential evapotranspiration data at daily time scale are required as inputs to compute streamflow at the watershed outlet. Since these regions are free from snow, snow routine is ignored in this study. Considering a semi – distributed model, areal averages of the climatological data are computed separately for each subbasin by a simple weighting procedure where the weights are determined by climatological and topographical considerations or by some geometric method like the Thiessen polygons. The climatological input is further corrected for elevation above sea level by constant lapse rates (Bergstr¨om, 1995). Beside geographical characteristics of the catchment the model has a number of parameters, values of which are estimated by calibration.

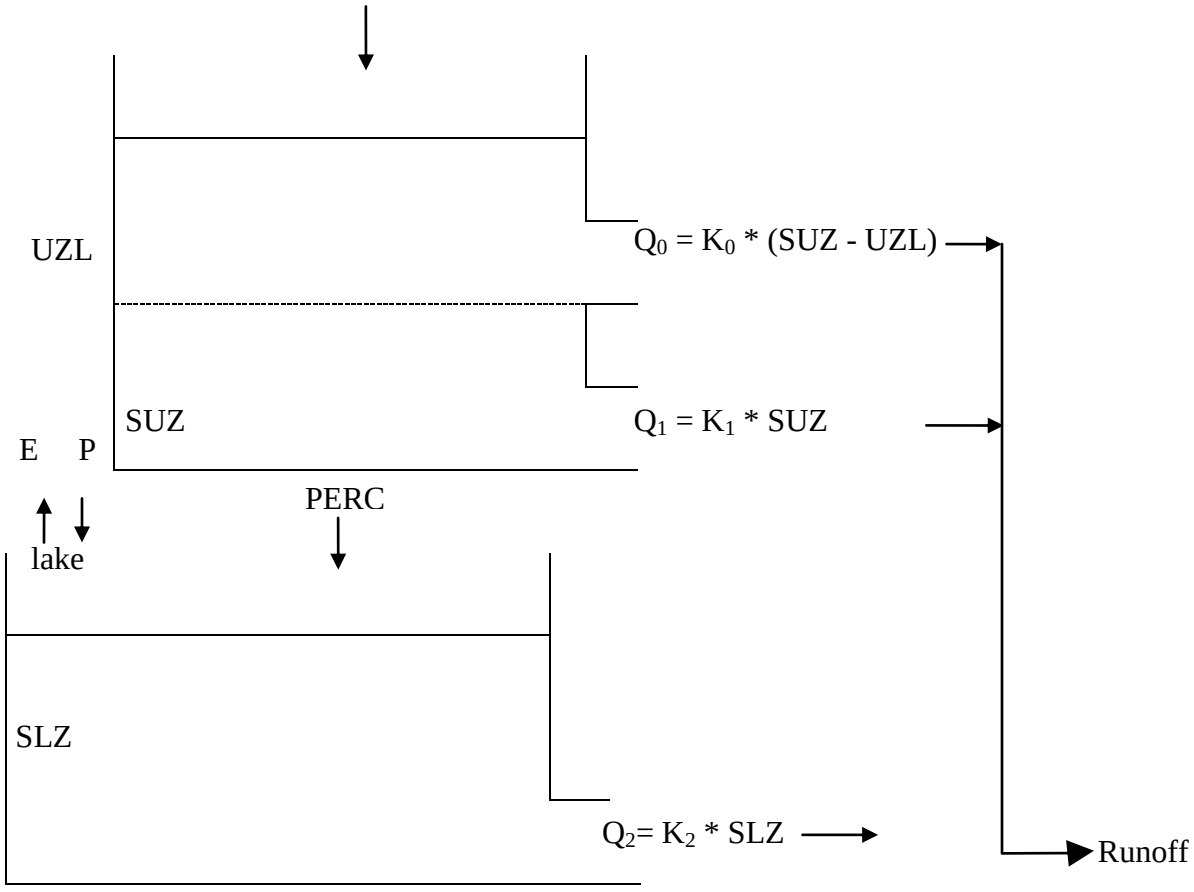

Fig. 4.4 Schematic of HBV model (Seibert, J., 1999).

4.3.2. Estimation of the model parameters

i. Soil routine

The soil moisture (S_{SOIL} (t)), which can range from zero (dry soil) to maximum field capacity (P_{FC}), is very important. The water content of soil affects the infiltration rate where higher water content increases the hydraulic conductivity and thus reduces the space availability for storage of infiltrating water causing different flow processes.

The soil moisture accounting routine controls the runoff generation (direct runoff, interflow, and actual evapotranspiration) based on three parameters: the maximum soil moisture storage (P_{FC}), the limit for potential evapotranspiration (P_{LP}), and the soil parameter (P_{BETA}). When P_{FC} is exceeded and the precipitation does not infiltrate anymore into the soil, the direct runoff is generated. The

water that infiltrated in the soil layer partly is captured by the soil and partly flows as the groundwater flux. Based on the amount of input to the soil (i.e. rainfall in this case) at a certain time step, I (t) (mm day^{-1}), the flux to the groundwater, F (t) (mm day^{-1}), is computed; the remaining part of P (t) is added to the soil box. The partition is a function of the ratio between current water content of the soil box (S_{SOIL}, mm) and its maximum field value (P_{FC}, mm) Eq. [4.1].

$$F\ (t) = I\ (t) \left(\frac{S_{SOIL}\ (t)}{P_{FC}} \right)^{P_{BETA}} \qquad [4.1]$$

Actual evapotranspiration from the soil box equals the potential evaporation if S_{SOIL}/P_{FC} is above P_{LP} P_{FC}, while a linear reduction is applied when S_{SOIL}/P_{FC} is below this value [Eq. 4.2]

$$E_{act} = E_{pot} \cdot \min \left(\frac{S_{SOIL}\ (t)}{P_{FC} \cdot P_{LP}}, 1 \right) \qquad [4.2]$$

The relation indicates that the interflow increases with increasing of SM and when infiltration doesn't occur, interflow is not generated. Parameter LP is the fraction of FC above which potential evapotranspiration occurs. The actual evapotranspiration ranges from zero when the soil is dry to the potential at some critical moisture content.

ii. Response function

The response function transforms the excess water from the soil moisture zone to runoff. Groundwater recharge is added to the upper groundwater box (S_{UZ}, mm). P_{PERC} (mm day^{-1}) defines the maximum percolation rate from the upper to the lower groundwater box (S_{LZ}, mm). Runoff from the groundwater boxes is computed as the sum of two or three linear outflow equations (P_{K0}, P_{K1}, AND P_{K2}, day^{-1}, depending on weather S_{UZ} is above a threshold value, P_{UZL} (mm), or not Eq. [4.3]).

$$Q_{GW}\ (t) = P_{K2} \cdot S_{LZ} + P_{K1} \cdot S_{UZ} + P_{K0} \cdot \max\ (S_{UZ} - P_{UZ}, 0) \qquad [4.3]$$

This runoff is finally transformed by a triangular weighting function defined by the parameter PMAXBUS Eq. [4.4].

$$Q_{sim}(t) = \sum_{i=1}^{P_{MAXBUS}} c(i)\, Q_{GW}(t-i+1),$$

$$where\ c(i) = \int_{i=1}^{i} \frac{2}{P_{MAXBUS}} - \left| u - \frac{P_{MAXBUS}}{2} \right| \cdot \frac{4}{P_{MAXBUS}^2}\, du. \qquad [4.4]$$

Besides the standard version several alternative model variants can be chosen in HBV-light. For instance, instead of the two outflow from the upper groundwater box, one non-linear outflow can be used Eq. [3.5]

$$Q_{GW}(t) = P_{K2} \cdot S_{LZ} + P_{K1} \cdot S_{UZ}^{1+P_{ALPHAA}} \qquad [4.5]$$

The structure of the groundwater boxes can also be changed. In the one-box variant there is only one groundwater box, with the upper two outflows being active only when the storage is above certain threshold values. In the three-box variant there are three linear – outflow boxes above each other, and there are two parameters determining the maximum flow rate down to the next box. In another variant the simulated recharge from the soil routine is divided into two parts based on a relative portion determined by one parameter. One part is added directly to a linear storage, whereas the other part is evenly distributed over a subsequent period of a certain number of time steps and added to a second, parallel linear storage. This latter variant has been useful in catchments with deeper groundwater flow pathways (Seibert, 2000; Seibert et al., 2010)

4.4. Model calibration

All rainfall – runoff hydrological models (lumped or distributed) are simple representation of the real world processes. Besides this, the lumped model parameter represents an average value over the entire watershed. As a result, the model parameters cannot be measured and have to determine through a model calibration. Calibration is a process in which parameter adjustment are made in order to simulate as closely as possible the hydrological behavior of the watershed. The goodness of fit is always determined by an objective function. A proper model calibration is necessary to consider a good fit between simulated and observed watershed runoff volume (water balance), the shape of the hydrograph, the peak flow, and the base flow. All these objectives are considered

during model calibration because a single objective function cannot establish a reasonable match between simulated and observed data.

4.4.1. Calibration of HBV model

The daily values of hydrological and meteorological data for the period of 2003 – 2008 were used to calibrate the HBV light model for the Birr watershed. Daily values of evapotranspiration data were available from one research center which located in east of study area. Kobold et al (2006), Andr´eassian et al. (2004) and Oudin et al. (2005a, b) shown very simple assumptions of areal potential evapotranspiration as input in the watershed model (the same average for all watersheds) yield similar results as improved estimates of areal potential evaporation. According to their

Table 4.2. Parameters and their ranges were used during the Monte Carlo simulations.

Parameter	Explanation	Unit	Minimum	Maximum
Soil and evaporation routine:				
FC	Maximum soil moisture Storage	mm	100	600
LP	Soil Moisture threshold for reduction of evaporation	−	0.3	0.7
B	Shape coefficient	−	1	4
Groundwater and response routine:				
K_0	Recession coefficient	d^{-1}	0.05	0.2
K_1	Recession coefficient	d^{-1}	0.01	0.2
K_2	Recession coefficient	d^{-1}	0.006	0.05
UZL	Threshold for K_0 outflow	mm	10.2	25.6
PERC	Maximum flow from upper to lower GW-box	mm $^{d-1}$	1.4	2.8
Routing routine:				
MAXBUS	Routing length of	d	1.5	2.9

conclusions we suppose that the estimates of areal evapotranspiration from one station did not have a significant influence on the efficiency of the model. Manual adjustments of the model parameters have been done following Monte Carlo simulations (MCS), in order to obtain a process-based representation of the hydrological characteristics in the watershed. The Monte-Caro procedure was run to evaluate the watershed response characteristics, and to discover physically realistic model's parameters ranges.

Wide ranges of possible values were set for each parameter based on ranges of calibrated values from other model applications (e.g., Bergström, 1990; Uhlenbrook et al, 2010), to define possible initial Monte-Carlo simulation parameter ranges as shown in Table 4.2 more than 400,000 parameter sets were generated for the watershed using random numbers from a uniform distribution within these ranges for each parameter on daily time steps.

4.5. Model performance statistics

The agreement between observed and computed runoff was evaluated by three main criteria of fit (IHMS, 1989): (a) visual inspection of the computed and observed hydrographs, (b) the absolute bias which measures the volumetric error :

$$abias = \frac{\left|\sum (Q_{com}(t) - Q_{obs}(t))\right|}{\sum (Q_{obs}(t)} \qquad [4.6]$$

Where Q_{com} is computed (simulated) streamflow, Q_{obs} observed streamflow, and (c) the coefficient of model efficiency, R_{eff} is normally used for assessment of simulations

$$R_{eff} = 1 - \frac{\sum (Q_{com}(t) - Q_{obs}(t))^2}{\sum (Q_{obs}(t) - \overline{Q_{obs}})^2} \qquad [4.6]$$

R_{eff} compares the prediction by the model with the simplest possible prediction, a constant value of the observed mean value over the entire period. *abias* value of zero indicates that there is no volumetric error while a value larger than zero indicates that there is under- or overestimation of the observed volume. R_{eff} =1 indicates a perfect match between the simulated and the observed flows.

CHAPTER FIVE

5. Result and Discussion

First we discussed the spatio-temporal rainfall variability over Birr watershed from newly deployed rain gauges we used the new rain gauge data as reference rainfall because it has better spatial representation than the existing gauges. We then discussed the comparison result of evaluation of the quality of daily rainfall measurements from existing rain gauges verses newly deployed rain gauges over the summer period of 2012. We also analyzed the rainfall representation of daily rainfall through streamflow predictive skills using rainfall inputs from existing and newly deployed rain gauges for summer period of 2012. Finally we discussed the comparison result between existing historical rain gauges and satellite rainfall products through direct average rainfall magnitude and streamflow predictive skills.

5.1. Spatio – temporal rainfall distribution of rainfall over Birr Watershed

We have used statistical methods to analyze the different aspects of spatial and temporal patterns of rainfall from newly deployed rain gauges over Birr watershed for the summer period of 2012. The statistics of hourly rainfall observations from newly deployed rain gauges are shown in the table 5.1. Statistics of the rainfall changed when no-rain hours were excluded from the analysis. For instance, without excluding the no-rain hours, the mean hourly rainfall for all stations were less than one, however after excluding no-rain hours, the mean rainfall varies from 1.6 mm to 3 mm where as standard deviation varies from 2.4 to 4. The percent duration of rainy hours of this study area varies from 19% to 25% which indicates that the frequency of hourly rainfall occurrence was small. Most of the stations on the high elevation areas of this watershed have higher percent of hourly rainfall duration than those on low-elevation. Station Feresbet is located at high altitude which has higher percent of rainfall duration and station Senbo are located at relatively low elevation with small percent of rainfall duration. The small percentage of rainfall duration suggests the presence of strong temporal variability of hourly rainfall. The diurnal variability of hourly rainfall indicates there are strong diurnal cycles in both frequency and intensity with maximum in the afternoon and minima in the morning for Birr watershed. Figure 5.1 shows the mean hourly accumulation of rainfall depth and coefficient of variation of various temporal scale rainfall depths for the period od summer 2012 over Birr watershed. The figure shows for the specified time period, maximum hourly

rainfall accumulation is observed at 15:00 and 20:00 local hour Birr watershed, the minimum hourly rainfall accumulation is observed at 11:00 local hour for Birr watershed. This result reveals

Table 5.1. Statistics of hourly rainfall observation

	Atiha	Gentabo	Makesegni	Amstegna	Dangber	Bahta	Senbo	Anjene	Feresbet	Zanbit	Dangbe
unconditional statistics											
Data (h)	2040	2040	2040	2040	2040	2040	2040	2040	2040	2040	2040
mean	0.50	0.45	0.45	0.37	0.31	0.50	0.43	0.49	0.60	0.50	0.39
STD	1.97	1.73	1.89	1.26	1.23	2.29	1.82	1.91	2.28	2.07	1.67
Conditional statistics											
Data (h)	436	452	405	450	388	416	406	493	462	409	400
mean	2.32	2.03	2.28	1.70	1.63	2.47	2.16	2.02	2.67	2.49	2.00
STD	3.74	3.21	3.72	2.23	2.41	4.56	3.60	3.46	4.18	4.04	3.31

that for this region, high frequency of rainfall occurrence is observed from the mid-day up to mid-night. Also the coefficient of variation (CV) indicates the presence of strong spatial variability in this region.

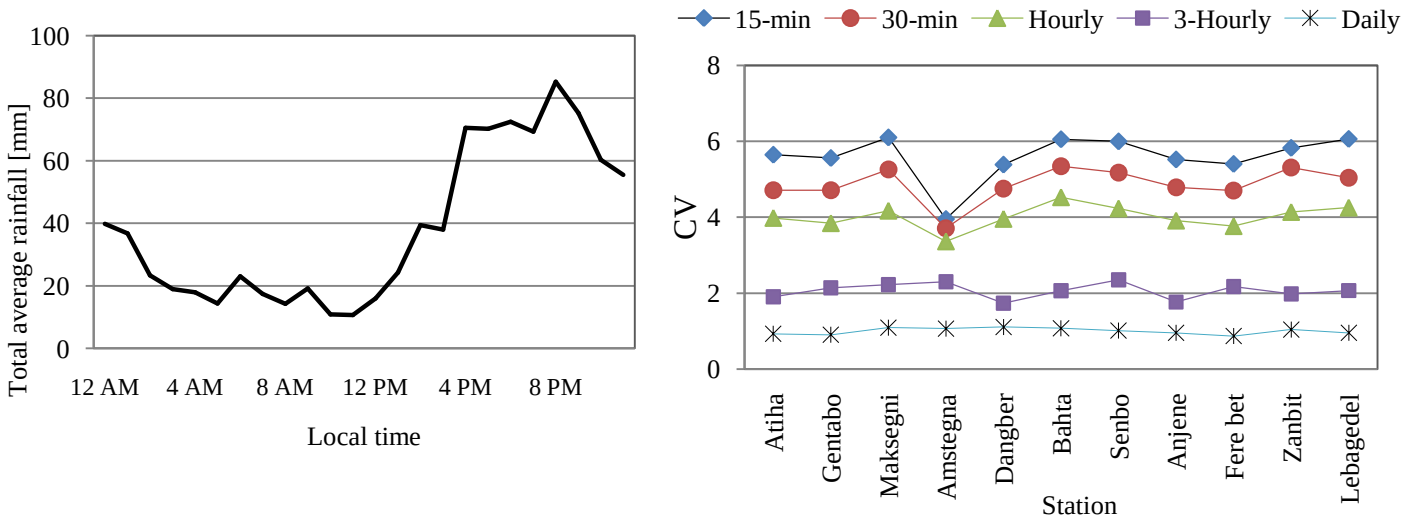

Fig. 5.1 Mean hourly accumulation (left) and coefficient of variation of various temporal scale rainfall depths (right) for the period of 08 July to 30 September 2012 for Birr watershed.

The CV increases as the resolution of rainfall depth increases. For all stations, it is observed that the CV is higher for 15-minute rainfall in the reverse small value of CV is observed for daily rainfall. The value of CV suggests that the temporal variability of rainfall is very high if the temporal resolution is high.

5.2. Newly deployed rain gauges verses existing rain gauges

In order to make use of the historical rain gauge data sets from the existing rain gauges, we evaluated the representativeness of the existing rain gauges using reference rainfall from recently deployed dense rain gauges in the watershed. We also assessed the representativeness of existing rain gauges through streamflow predictive skills (not shown here) for the summer period of 2012 (II). We used new rain gauge data as reference rainfall because it has better spatial representation than the existing gauges. The result revealed the existing rain gauges show only 5% underestimation of the accumulated depth of rainfall for the period of 08 July to 30 September 2012 (i.e. 85 days) figure 5.2. This results show that the existing rain gauges provide fairly representative rainfall amount at daily and seasonal time span. Therefore, we used the historical data set to evaluate the accuracy of satellite rainfall estimates.

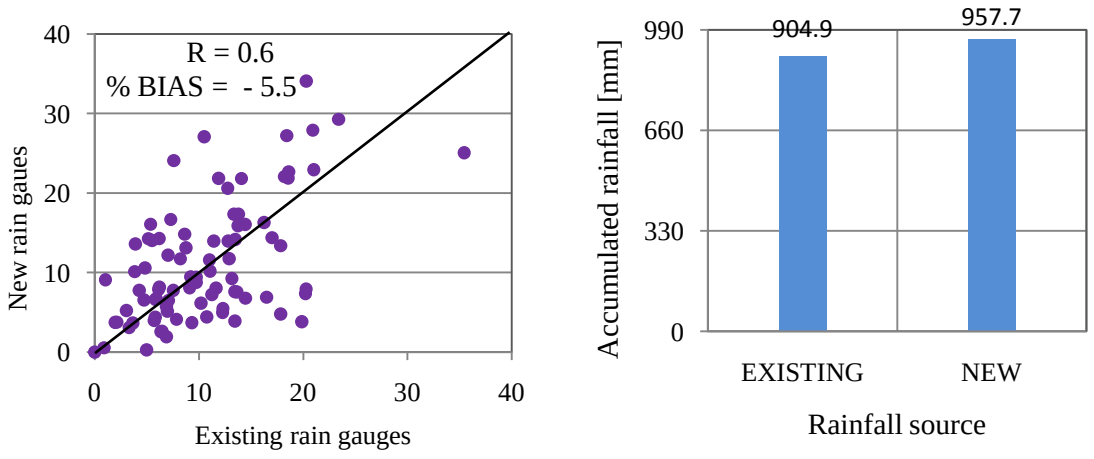

Fig. 5.2 Scatter plot of daily rainfall (left) and accumulated rainfall from newly deployed rain gauges and existing rain gauges.

5.3. Satellite rainfall products versus rain gauges

To better understand the impacts of rainfall inputs on the output of model, we begin by comparing watershed – averaged rainfall magnitudes derived from satellite rainfall products (i.e. 3B42RT, 3B42V7, and 3B42V6) and rain gauge that have been used in subsequent HBV – light modeling for Birr watershed. The comparison performed for the study period of 2003 – 2008, corresponding to HBV – light calibration period at Birr watershed (see figure 3.1). The direct intercomparison of rainfall products was based on Thiessen Polygon interpolated average rainfall over the watershed. We point out that while direct intercomparison of the satellite rainfall products is meaningful as the products represent average rainfall extracted from each grid that lies in the watershed based on its weight.

Figure 5.3 (a) clearly shows, In general, the interannual variation of rain observed by rain gauges were captured by all satellite rainfall products, except 3B42V6, fails to capture from year 2004 to 2005, when rain gauges reported an increase of annual rainfall from the year 2004 (1187.9 mm) to 2005 (1288.1 mm), but 3B42V6 reported a drop in annual rainfall from year 2004 (1031.2 mm) to 2005 (619.8). In addition to this, 3B42V6 highly underestimates the annual rainfall for the whole study period. The new version TMPA 3B42V7 products shows better performance in capturing interannual variation of rainfall compared to other. For majority of the months, 3B42RT and 3B42V7 satellite rainfall products showed similar performance and gave small overestimation, while 3B42V6 consistently gave the largest underestimation. The mean rainfall observed at rain gauge comparatively equal to 3B42RT (i.e. 1353 mm for rain gauge & 1358 mm for 3B42RT), while 1429 mm for 3B42V7 but its highly underestimated by 3B42V6 (only 812 mm) for the study period. Analyzing the seasonal rainfall variation was very important since this study area is characterized by only one rainy season (mono-modal) which lasts from June to end of September (JJAS). The seasonal rainfall comparison result revealed that on average more than 70 % of annual rainfall occurs in the summer rainy season (JJAS) for the same study period as observed from rain gauge. The percentage of seasonal rainfall variation observed at rain gauge was approximately similar to new research version TMPA 3B42V7 products Figure 5.3 (b), while the real time version 3B42RT & 3B42V6 underestimates the seasonal rainfall; however it's large of 3B42V6.

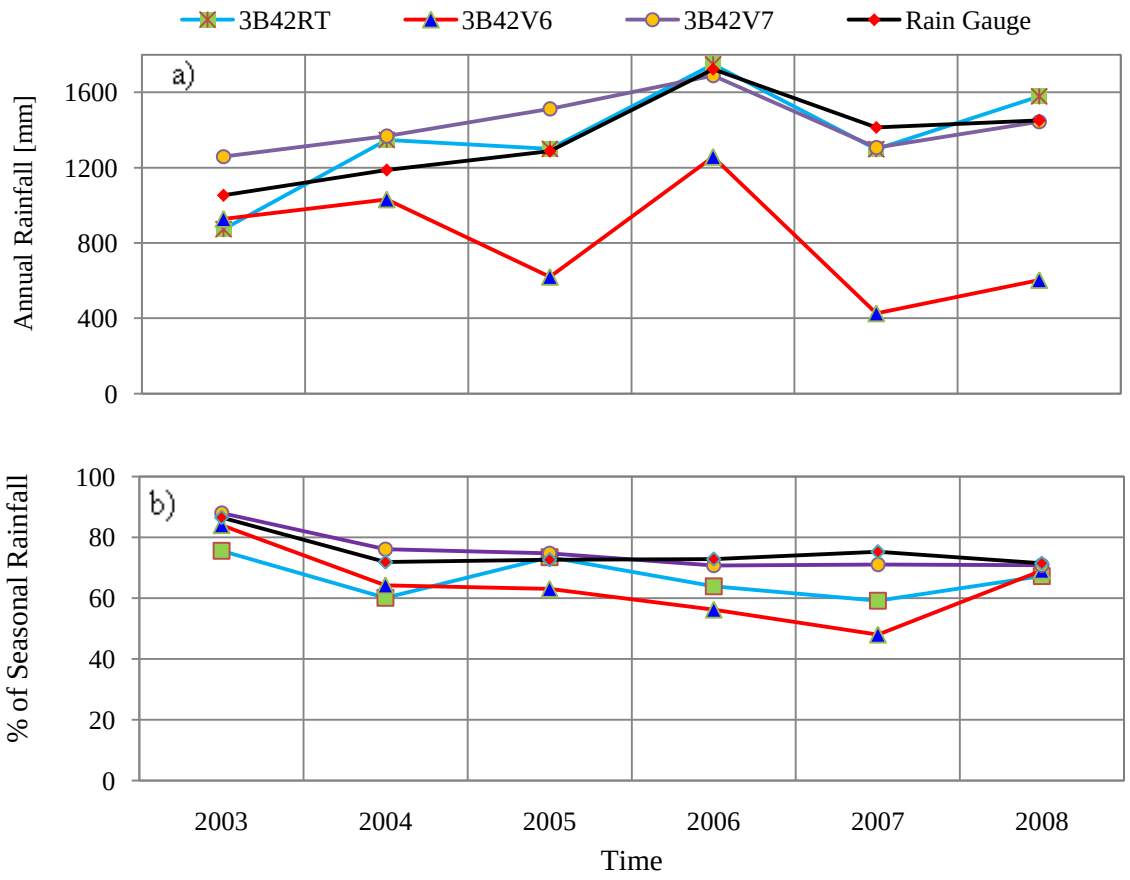

Fig. 5.3 Annual (a) and percentage of seasonal (b) rainfall (i.e. JJAS: June, July, August, and September) from various rainfall products for the period of 2003 – 2008.

Figure 5.4 shows monthly and mean monthly rainfall analysis from various rainfall products. The trend of monthly rainfall observed at rain gauges captured by all satellite rainfall products except for April 2004 where unusual overestimation was observed by 3B42RT products. The monthly peak rainfall observed by rain gauge was underestimated in the range of 31 % to 85 % by 3B42V6 for the whole study period, more than 40 % in year 2003, 2007 by 3B42RT, and comparatively small for 3B42V7 only by less than 20 % for year 2003, 2004 and 2007. In year 2005 3B42V7 overestimated the monthly peak by more than 60 %, while 3B42RT by more than 25 % for year 2005 and 2008. The monthly peak rainfall observed by rain gauge lags by a month for year 2003 and 2007 compared to satellite rainfall products, while it occurs in the same month for year 2004 and 2005.

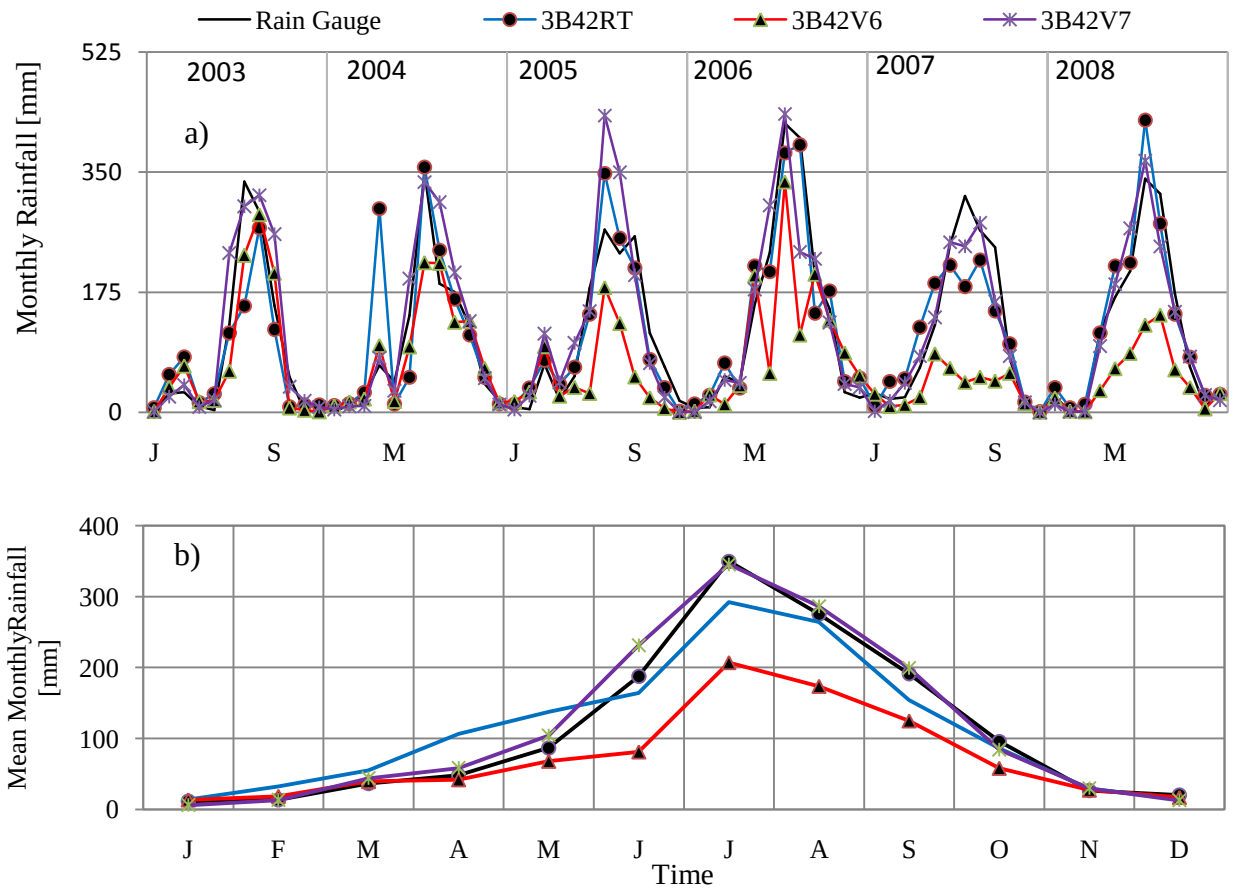

Fig.5.4 Monthly (a) and mean monthly (b) rainfall over Birr watershed obtained from rain gauge data and various satellite rainfall products for the period of 2003-2008.

The mean monthly peal rainfall occurs in July month for all rainfall products. Compared to rain gauges values, 3B42V6 satellite rainfall products underestimated the peak mean monthly rainfall by 41 %, 3B42RT by 11 %, while 3B42V7 approximately accurately estimates the peak mean monthly rainfall figure 4 (b).

Figure 5.5 presents intercomparison of daily rainfall estimates. The comparison statistics (R = Pearson's correlation coefficient) are given in each plot. Correlations between satellite rainfall values and rain gauge values were fair at 0.4 – 0.51 when compared to correlation between satellite rainfall values. Poor correlation was observed between rain gauge and 3B42V6 (R = 0.4). The result was improved compared to (Betaw and Gebermichael., 2011), who compared daily satellite rainfall products with daily rainfall value derived from one rain gauge in the grid, which suggests the need of dense rain gauge network to capture average rainfall in the grid.

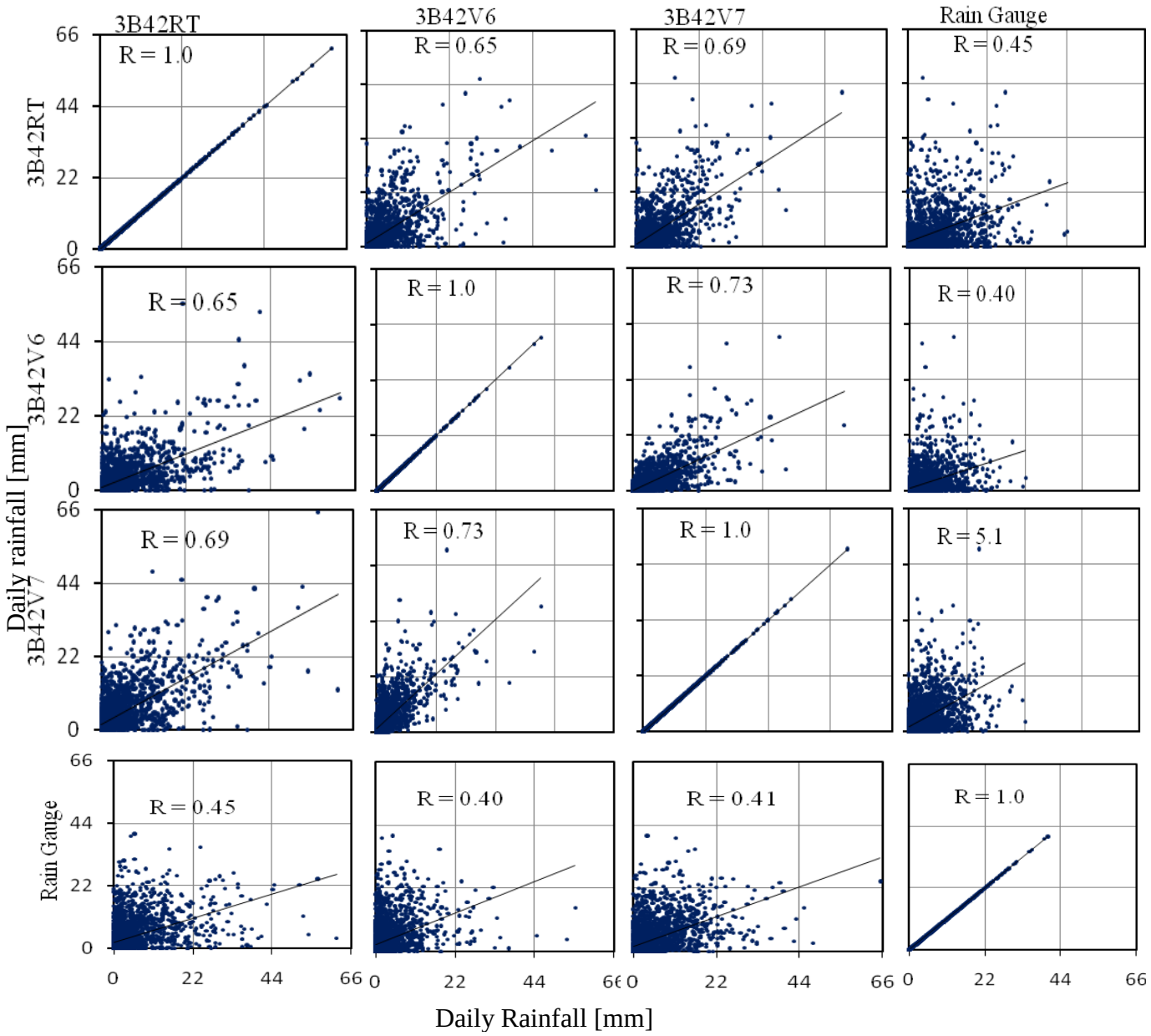

Fig. 5.5 Intercomparison of daily rainfall from satellite rainfall products (i.e. 3B42RT, 3B42V6, 3B42V7) and rain gauge for Birr watershed for the period of January 2003 – December 2008.

Correlations between pairs of daily satellite rainfall values were modest at 0.65 – 0.73, with the highest correlation observed between 3B42V6 and 3B42V7 (R = 0.73), also high correlation observed between 3B42RT and 3B42V7 (R = 0.69).

Figure 5.6 presents intercomparison of monthly rainfall estimates. At monthly time scale, the correlation between rain gauge and satellite rainfall values was higher than correlation between

satellite rainfall values. Correlations between monthly satellite rainfall values and rain gauge values were high at 0.76 – 0.93, which is even higher than the correlation between satellite monthly rainfall values. The highest correlation was observed between rain gauge and 3B42V7 (R = 0.93) where as the lowest between 3B42V6 and rain gauge (R = 0.76). The correlations between monthly satellite rainfall values was at 0.7 – 0.87, high between 3B42RT and 3B42V7 (R = 0.87), medium between 3B42V6 and 3B42V7 (R = 0.80) and poor between 3B42RT and 3B42V6 (R = 0.70).

From the above comparison analysis, it's revealed that both new version 7 TMPA 3B42RT and 3B42V7 rainfall estimates gave reasonably accurate result. The result revealed that in this watershed, 3B42RT accurately estimated the total average rainfall with negligible % bias, this result is also consistent with findings in northwest region of Ethiopia (Romilly and Gebremichael., 2011) but underestimated the seasonal rainfall with % bias less than - 11 %; while very small overestimation of average seasonal and total rainfall observed in 3B42V7 rainfall estimates with % bias less than 6%. However; version 6 TMPA 3V42V6 rainfall estimates consistently underestimated both the total and seasonal rainfall with % bias greater than – 40%. There have been subsequent studies that conducted in Blue Nile River basin to evaluate satellite rainfall products in the estimation of rainfall, Bitew and Gebremichael., 2010, Romilly and Gebremichael (2011), and Dinku et al. (2010); based on their studies and the result of this study, its concluded that 3B42RT and 3B42V7 are much closer to the actual rainfall fields in Ethiopian highlands compared to 3B42V6. It is exciting to note that the new upgraded post – real – time version 7 TMPA product (3B42V7), which provides a variety of improvements with modernize the input data sets and correct several issues, was more accurate than the previous post – real – time version 6 TMPA product (3B42V6).

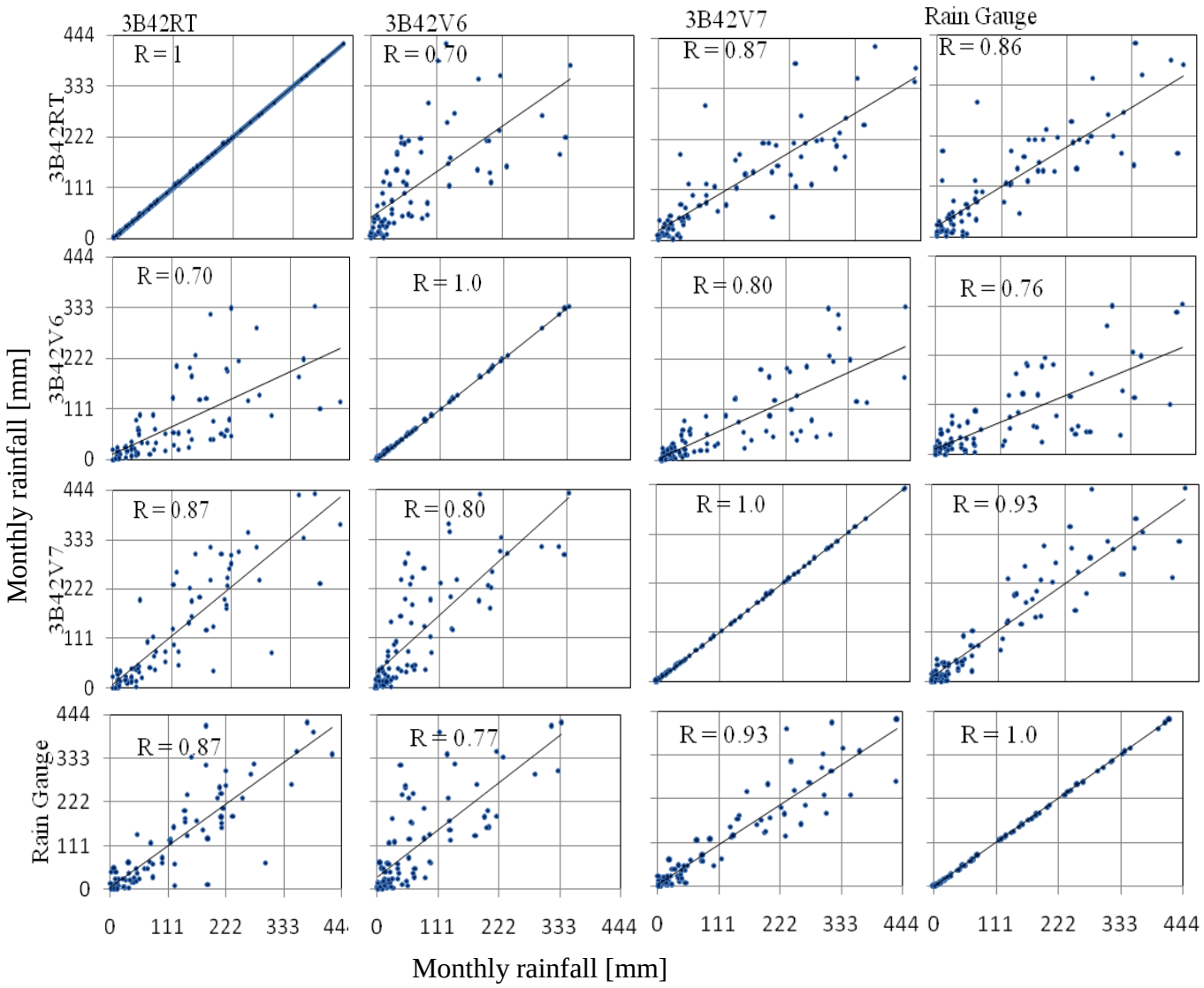

Fig. 5.6 As in Fig.5. 5, but for monthly rainfall.

5.4. Model parameter calibration result

The daily values of hydrological and meteorological data for the period of 2003 – 2008 were used to calibrate HBV – light model for the Birr watershed with the time step of one day. While 5 to 10 years of daily data are normally sufficient to calibration of HBV – light model (Bergstrom, 1995), we used one year (2003) for warm up period and 5 year for simulation period. The model parameter calibration was done as discussed in section 4.4; there a number of parameter sets that yields a good agreement between observed and simulated streamflow and NSE = 0.70 since the value of one

parameter was compensated by other parameter value. Table 5.2 shows the parameter values that are used in the simulation of satellite based rainfall inputs.

Generally, it's observed that there was an overall agreement between simulated and observed hydrographs, even if the simulated flows underestimated the observed peak flow for some year. The observed and simulated exceedance probability curves were close to each other for the majority parts; except very slight underestimation (less than 5 % of exceedance probability) of simulated peak flow. The model performance statistics (NSE = 0.70, R = 0.71, and bias = -2.56 %) indicate that the calibration results can be considered satisfactory as compared to other HBV applications at daily time scale (e.g., Uhlenbrook et al. 2010). Figure 5.7 presents the comparison of model simulation using rainfall input from rain gauge with observed daily streamflow for the calibration period in terms of a time series plot and an exceedance probability plot.

Table 5.2: HBV – light model parameter values obtained by calibrating HBV – light with rainfall input from rain gauge for the calibration period January 2003 – December 2008.

Parameter	Explanation	Unit	Parameter value obtained
Soil and evaporation routine:			
FC	Maximum soil moisture storage	mm	105
LP	Soil Moisture threshold for reduction of evaporation	−	0.80
β	Shape coefficient	−	2.7
Groundwater and response routine:			
K_0	Recession coefficient	d^{-1}	0.30
K_1	Recession coefficient	d^{-1}	0.20
K_2	Recession coefficient	d^{-1}	0.10
UZL	Threshold for K_0 outflow	mm	14
PERC	Maximum flow from upper to lower GW-box	$mm\ ^{d-1}$	3.0
Routing routine:			
MAXBUS	Routing length of weighting function	d	1.056

5.5. Satellite rainfall simulation of streamflow

The purpose of these simulations was to assess the performance of satellite rainfall estimates on streamflow simulation capability when HBV – light was calibrated with rain gauge data. We simulated daily streamflow for the calibration period (2003 – 2008) allowing one year (2003) for warm – up period using various rainfall inputs separately in calibrated HBV model. Figure 5.8 presents the comparison of model simulation using rainfall input from various rainfall inputs (i.e. rain gauge, 3B42RT, 3B42V7, and 3B42V6) with observed daily streamflow for Birr watershed.

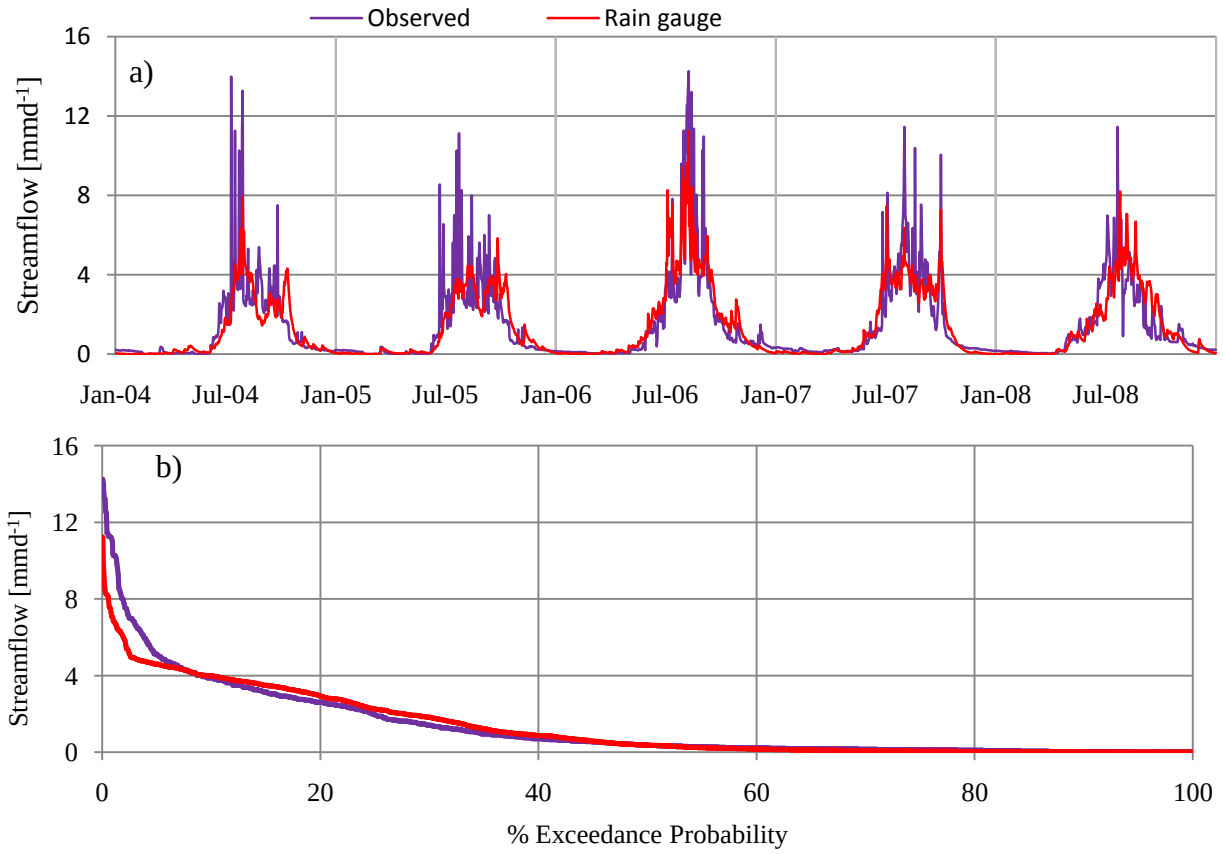

Fig. 5.7 Comparison of HBV-light simulated streamflow (based on rain gauge data input) and observed daily streamflow, during the calibration period, in terms of (a) time series and (b) exceedance probabilities.

Simulation from all rainfall inputs captured the overall shapes of observed hydrograph with slight underestimation of large flood events in the rain gauge & 3B42V6 (for all simulation period), 3B42RT & 3B42V7 (for year 2006 to 2007) based simulation, however; the degree of underestimation of large flood events was very small for rain gauge and 3B42RT rainfall inputs,

worse for 3B42V6. Model simulations underestimated the largest flood events with exceedance probabilities of 0.77 % or less for those with rain gauge and 3B42RT rainfall inputs, and of 2 % or less for 3B42V6 rainfall inputs. Simulation based on 3B42V7 gave reasonably accurate streamflow simulation for large flood events. 3B42RT simulation resulted in unexpected simulation value of streamflow in April – 2004 (figure 5.8); it's mainly because of overestimation of rainfall in same period (April – 2004) figure 5.4. In general; rain gauge, 3B42RT, and 3B42V7 simulations of streamflow exhibited similar performance in simulation of daily streamflow; 3B42V7 simulation slightly showed better performance in simulating large flood events.

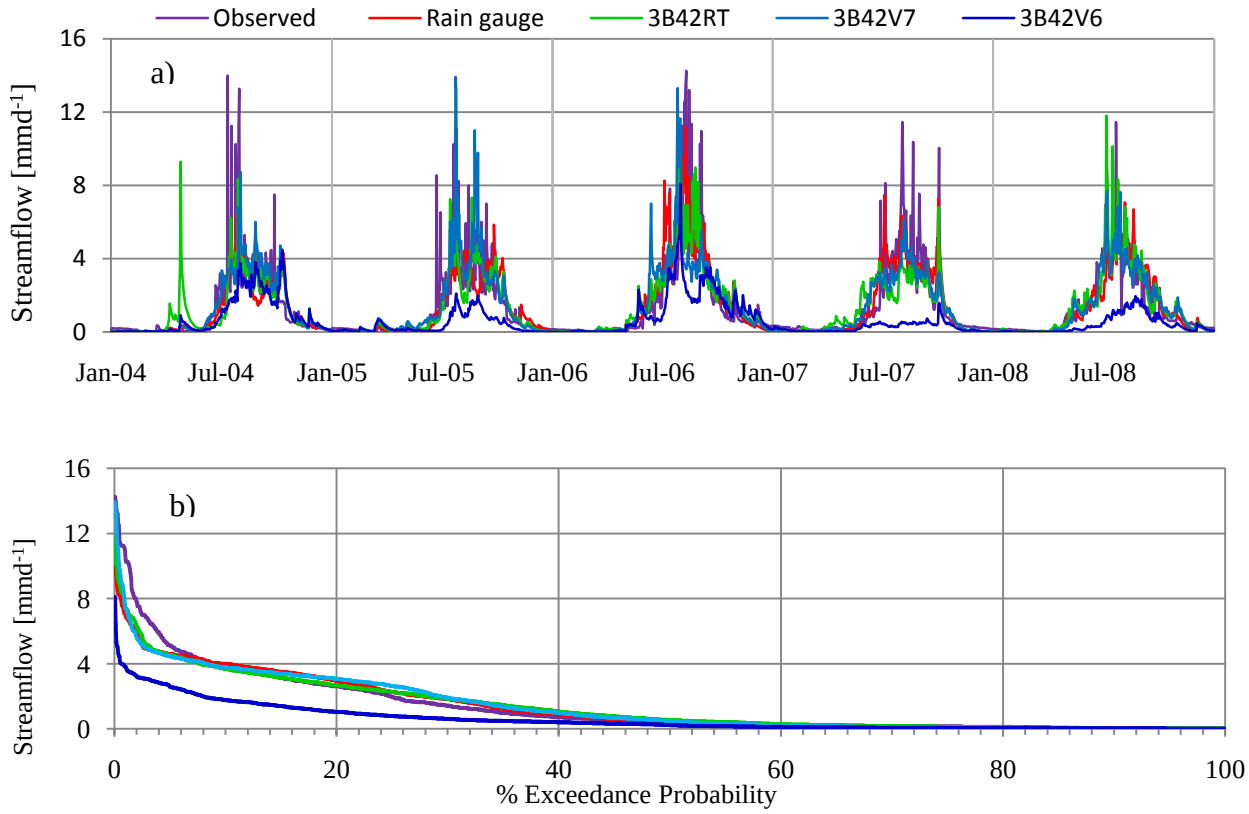

Fig. 5.8 Comparison of HBV-light simulated streamflow (based on rainfall input data from various sources in the legend) and observed daily streamflow, during the calibration period, in terms of (a) time series and (b) exceedence probabilities.

Figure 5.9 shows the statistical comparisons of simulations of HBV – light model from various rainfall inputs. Simulations of streamflow from rain gauge, 3B42RT, and 3B42V7 inputs had showed comparatively similar performance, while simulation based 3B42V6 inputs resulted in large negative bias and small NSE value. Simulation based on rain gauge has relatively high NSE (0.708) and r^2

(0.71) values. Simulation based on 3B42RT and 3B42V7 has nearly similar NSE and r^2 value (0.6 & 0.6 for 3B42RT and 0.57 & 0.59 for 3B42V7) respectively. Small value of biases were observed in the simulations based on rain gauge (% BIAS = - 2.5 %), 3B42V7 (% BIAS = 1.3 %), and 3B42RT (negligible bias). There were very small values of NSE (0.18), r^2 (0.33) and large negative bias (%BIAS = -55.6 %) in 3B42V6 based simulation of streamflow.

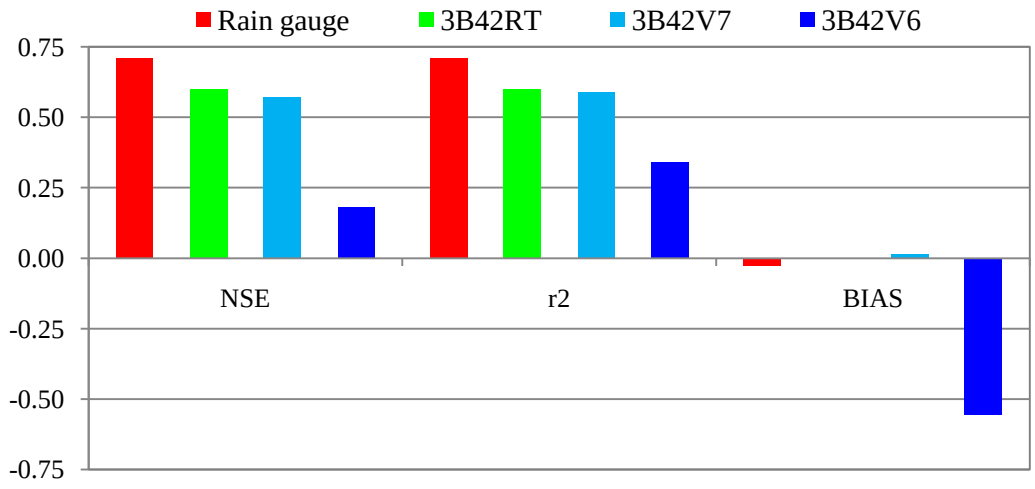

Fig.5.9 Statistical comparison of simulations of daily streamflow based on various rainfall inputs indicated in the legend.

Figure 5.10 presents the intercomparison of model simulation based on various rainfall inputs using Pearson correlation coefficients (R). High correlation value observed between observed and simulation based on rain gauge rainfall inputs compared to simulation based on satellite rainfall inputs. This result revealed that the same correlation value (R = 0.77) observed between simulations based on 3B42RT and 3B42V7 rainfall inputs compared to observed streamflow whereas the correlation between observed and 3B42V6 based simulation were poor (R = 0.58). The highest correlation value was observed between model simulations from satellite rainfall inputs. Simulations based on 3B42RT and 3B42V7 rainfall inputs were highly correlated (R =0.89), and relatively simulation based on 3B42RT and 3B42V6 rainfall inputs were moderate (0.72). In general, good correlation value observed between simulation based on rain gauge rainfall inputs and simulations based on satellite rainfall inputs. Simulations based on 3B42RT and 3B42V7 rainfall inputs gave nearly same correlation value (R = 0.86 for 3B42RT and R = 0.84 for 3B42V7) compared to rain gauge based simulation.

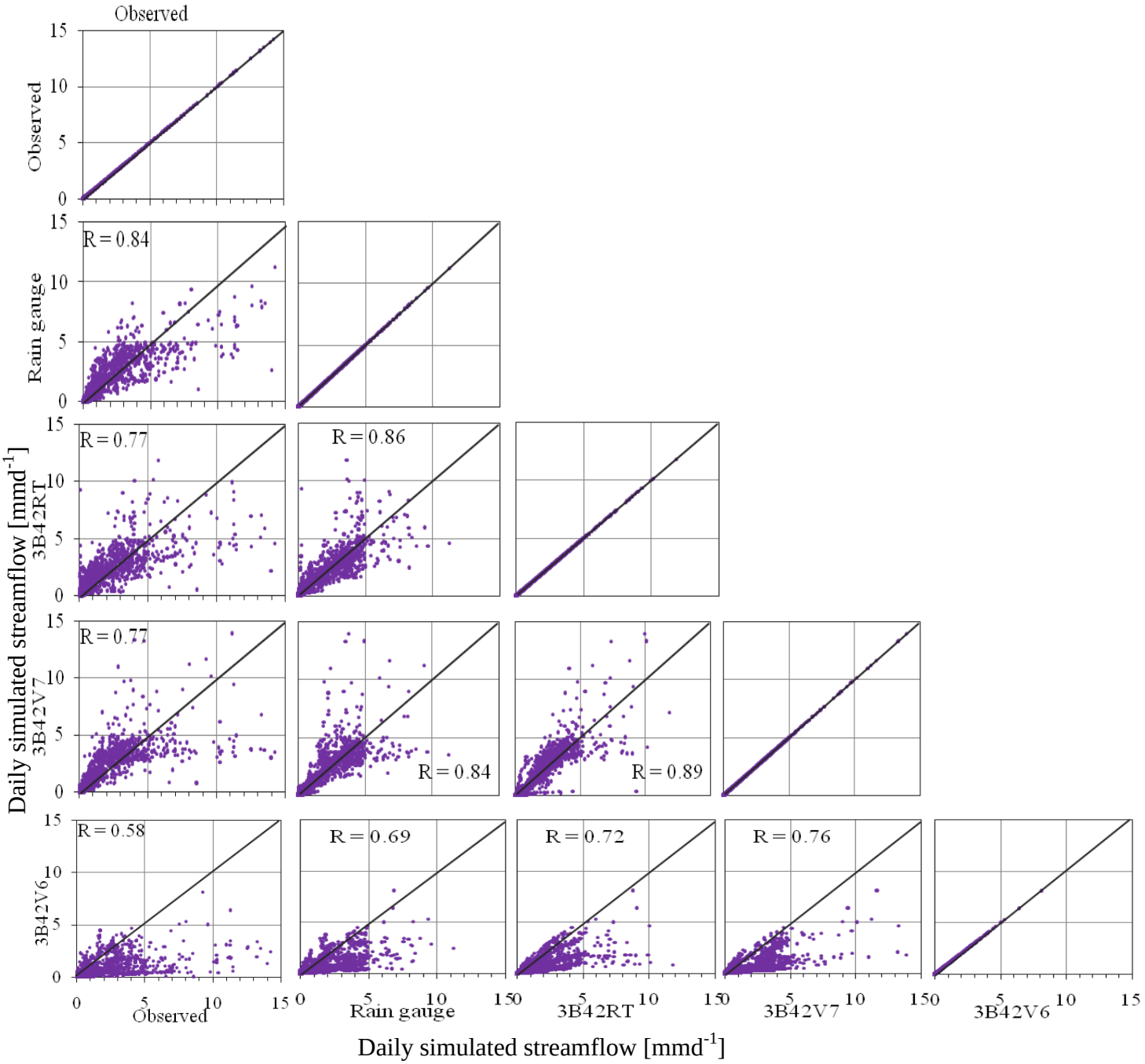

Fig. 5.10 Intercomparison simulated daily streamflow (based on 3B42RT, 3B42V6, 3B42V7, and rain gauge rainfall input data) and observed daily streamflow, the period of Jan, 2003 – Dec, 2008.

CHAPTER SIX

6. Conclusion

This study involves deployment of dense rain gauges over Birr watershed for high quality rainfall data collection over the summer period 2012, collection of historical rainfall data from existing rain gauges, satellite rainfall products and observed streamflow measurements and application of HBV hydrological model to simulate streamflow. The rainfall data sets and the modeling activities were used to characterize and determine uncertainty in input precipitation data; high resolution satellite rainfall estimates in this case. In order to make use of the historical rain gauge data sets from the existing rain gauges, we evaluated the representativeness of the existing rain gauges using reference rainfall from recently deployed dense rain gauges in the watershed. We also assessed the representativeness of existing rain gauges through streamflow predictive skills. The result revealed that the existing rain gauges show only 5% underestimation of the accumulated depth of rainfall. We can conclude from this result, the existing rain gauges provide fairly representative rainfall amount at daily and seasonal time span. Therefore, we used the historical data set to evaluate the accuracy of satellite rainfall estimates.

The comparison results of rainfall magnitudes from satellite rainfall products and rain gauges revealed that both new version 7 TMPA 3B42RT and 3B42V7 rainfall estimates gave reasonably accurate result compared to rain gauge rainfall estimates. The result revealed that, in this region, 3B42RT accurately estimated the total average rainfall with negligible bias, but underestimated the seasonal rainfall with % bias less than - 11 %; while very small overestimation of average seasonal and total rainfall observed in 3B42V7 rainfall estimates with % bias less than 6%. However; version 6 TMPA 3V42V6 rainfall estimates consistently underestimated both the total and seasonal rainfall with % bias greater than – 40%. Based on subsequent studies conducted in Blue Nile River basin to evaluate satellite rainfall products in the estimation of rainfall and the result of this study, its concluded that 3B42RT and 3B42V7 are much closer to the actual rainfall fields in Ethiopian highlands compared to 3B42V6. It is exciting to note that the new upgraded post – real – time version 7 TMPA product (3B42V7), which provides a variety of improvements with modernize the input data sets and correct several issues, was more accurate than the previous post – real – time

version 6 TMPA product (3B42V6) suggesting rainfall estimates based on TMPA 3B42V6 can't be a replacement of rain gauge measurements in this region.

This study showed the performance of satellite simulated streamflow when each of satellite rainfall data sets are used as an input to rain gauge calibrated HBV – light model. Simulation from all rainfall inputs captured the trend of observed hydrograph with slight underestimation of large flood events. Simulation based on the new version 7 of TMPA 3B42RT and 3B42V7 gave reasonably accurate streamflow simulation for large flood events compared to others. In general; simulation based on 3B42RT and 3B42V7 rainfall inputs exhibited similar performance in simulation of daily and monthly streamflow. On the other hand, the 3B42V6 streamflow shows poor performance which underestimates the large monthly flood events by greater than 75 %. This type of results was observed by previous researches, such as Bitew and Gebremichael (2010) in Ethiopian highlands. The study demonstrated that HBV – light model can be used to study the uncertainty in satellite rainfall inputs. This paper supports these previous findings and highlights the need of high quality streamflow data. We recommend dense rainfall measurement and stage – discharge rating curves should be given priority to improve the comparison result.

Reference

Andr´eassian, V., Perrin, C., and Michel, C.: Impact of imperfect potential evapotranspiration knowledge on the efficiency and parameters of watershed models, J. Hydrol., 286, 19– 35, 2004.

Arnold, J. G., Srinivasan, R., Muttiah, R. S., and Allen, P. M.: Large-Area Hydrologic Modeling and Asssessment: Part I. Model Development, J. Am. Water Resour. Assoc., 34(1), 73– 89, doi:10.1111/j.1752-1688.1998.tb05961.x, 1998.

Beighley. R. E., R. L. Ray,Y. He, H. Lee, L. Schaller, K. M. Andreadis, M. Durand, D. E. Alsdorf and C. K. Shum. Comparing satellite derived precipitation datasets using the Hillslope River Routing (HRR) model in the Congo River Basin Hydrol. Process. **25**, 3216–3229 (2011).

Bergström, S. Parametervärden för HBV-modellen i Sverige, Erfarenheter från modelkalibreringar under perioden 1975-1989 (Parametervalues for the HBV model in Sweden, in Swedish), SMHI Hydrologi, No.28, Norrköping, 35 pp, 1990.

Bergström, S. The HBV model - its structure and applications, SMHI Hydrology, RH No.4, Norrköping, 35 pp, 1992.

Bergstr¨om, S.: The HBV model (Chapter 13), in: Computer Models of Watershed Hydrology, edited by: Singh, V. P., Water Resources Publications, Highlands Ranch, Colorado, USA, 443– 476, 1995.

Bitew, M. M., and M. Gebremichael: Assessment of satellite rainfall products for streamflow simulation. Hydrol. Earth Syst. Sci., 15, 1147–1155, 2011

Betson, R. P., and Marius, J. B. Source area of strom runoff. Water Resources Research, Vol 5, No, 3,574-582, 1969.

Clemens, M. and Bumke, K. A comparison of precipitation in - situ measurements and model predictions over the Baltic Sea Area. Physics and chemistry of the Earth, part B: hydrology, Oceans and Atmosphere 26 (5-6): 437-442, 2001.

Dune, T. Relation of field studies and modeling in the prediction of storm runoff. Journal of Hydrology, Vol 65, 24-48, 1983.

Ebert, E. E.: Methods in verifying satellite precipitation estimates, in: Measuring Precipitation from Space: EURAINSAT and the Future, edited by: Levizzani, V., Bauer, P., and Turk, F. J., Adv. Glob. Change Res., 28, 611–653, Springer, Dordrecht, Netherlands, 2007.

Engida. A. N., M. EstevesCharacterization and disaggregation of daily rainfall in the Upper Blue Nile Basin in Ethiopia. Journal of Hydrology 399 (2011) 226–234, 2011.

Gebremichael, M., Krajewski, W. F., Morrissey, M., Huffman, G., and Adler, R.: A detailed evaluation of GPCP one-degree daily rainfall estimates over the Mississippi River Basin, J. Appl. Meteorol., 44(5), 665–681, 2005.

GES DISC. Goddard Earth Sciences, Data and Information Services Center. TRMM, Tropical Rainfall Measuring Mission. http:// trmm.gsfc.nasa.gov/data_dir/data.html, 2006.

Haile, A, T., Rientjes, T.,and Reggiani, P. Model sensitivity to rainfall representation: the representative elementary watershed, Water Resource Research, 2009.

Huffman, G. J., Adler, R. F., Bolvin, D. T., Gu, G., Nelkin, E. J., Bowman, K. P., Hong, Y., Stocker, E. F., and Wolff, D. B.: The TRMM Multi-satellite Precipitation Analysis (TMPA): Quasiglobal, multiyear, combined sensor precipitation estimates at fine scales, J. Hydrometeorol., 8(1), 38–55, 2007.

Isaaks, E. H. and R. Mohan Srivastava. Introduction to applied geostatistics. New York etc., Oxford University Press 1989.

JAXA, Japan Aerospace Exploration agency. TRMM data users hand book, 2006.

Leavesley, G.H., Litchy, R.W., Troutman, B.M., Saindon, L.G. Precipitation-Runoff Modeling System: User's Manual. US Geological Survey Water Resources Investigative Report, Denver, Colorado, 83–4238, 1983.

Legessea. D, Christine V. C., Franc¸oise G. Hydrological response of a catchment to climate and land use changes in Tropical Africa: case study South Central Ethiopia. Journal of Hydrology 275 (2003) 67–85 2003.

Linsley, R.K., Kohler, M. A., and Paulhus, J. L. H. Hydrology for engineers. McGraw-Hill, New York, 1958.

Lindstr¨om, G. and Bergstr¨om, S.: Improving the HBV and PULSEmodels by use of temperature anomalies, Vannet i Norden, 16– 23, 1992.

Lindstr¨om, G., Johansson, B., Persson, M., Gardelin, M., and Bergstr¨om, S.: Development and test of the distributed HBV-96 hydrological model, J. Hydrol., 201, 272–288, 1997.

Kobold, M., and Brilly, M. The use of HBV model for flash flood forecasting. Nat. Hazards Earth Syst. Sci., 6, 407–417, 2006.

NASA/ GSFC. National Aeronautics and space Administration / Goddard Space Flight Center.

O'Connell,P.E. Recent advances in the modeling of hydrological systems. Kluwer, Dordrecht, 3-30, 1991.

Ragan, R.M. An experimental investigation of partial area contributions. Int. Assoc. of Science Hydrology, No76, 241-251, 1968.

Oudin, L., Michel, C., and Anctil, F.: Which potential evapotranspiration input for a lumped rainfall-runoff model? Part 1-Can rainfall-runoff models effectively handle detailed potential evapotranspiration inputs?, J. Hydrol., 303, 275–289, 2005a.

Oudin, L., Hervieu, F., Michel, C., Perrin, C., Andr´eassian, V., Anctil, F., and Loumagne, C.: Which potential evapotranspiration input for a lumped rainfall-runoff model? Part 2-Towards a simple and efficient potential evapotranspiration model for rainfall-runoff modeling, J. Hydrol., 303, 290–306, 2005b.

Romilly, T. G. and Gebremichael, M. Evaluation of satellite rainfall estimates over Ethiopian river basins. Hydrol. Earth Syst. Sci., 15, 1505–1514, 2011

Seibert, J. HBV light, User's manual, Uppsala University, Institute of Earth Science, Department of Hydrology, Uppsala, 1996.

Seibert, J. Conceptual runoff models - fiction or representation of reality? Acta Univ. Ups., Comprehensive Summaries of Uppsala Dissertations from the Faculty of Science and Technology 436. 52 pp. Uppsala. ISBN 91-554-4402-4, 1999.

Seibert, J. Multi - criteria calibration of a conceptual runoff model using a genetic algorithm, Hydrol. Earth Syst. Sci., 4, 215–224, doi:10.5194/hess-4-215-2000, 2000.

Seibert, J. and McDonnell, J. J.: Land-cover impacts on streamflow: a change-detection modeling approach that incorporates parameter uncertainty, Hydrolog. Sci. J., 55, 316–332, doi:10.1080/02626661003683264, 2010.

Uhlenbrook, S., Mohamed, Y., and Gragne, A.S. Analyzing catchment behavior through catchment modeling in the Gilgel Abay, Upper Blue Nile River Basin, Ethiopia. Hydrol. Earth Syst. Sci., 14, 2153–2165, 2010. doi:10.5194/hess-14-2153-2010

WMO. Hydrological models for water-resources system design and operation: Operational Hydrology Report No. 34, WOM-No 740, 1989.

Zhong L.; L. Chiu, H. Rui, W. Teng, G. Serafino. Online Analysis and Visualization of TRMM and Other Precipitation Data Sets. GSFC Earth sciences Data and Information Services Center Distributed Active Center NASA/Goddard Space flight Center, Greenbelt Maryland, USA.

Appendices

Appendix I List of tables

Comparison result of average rainfall magnitude over the watershed.

Table 1: Annual rainfall from various rainfall products

Date	3B42RT	3B42V6	3B42V7	Rain Gauge
2003	873.9	928.6	1259.8	1053.8
2004	1347.9	1031.2	1367.6	1187.9
2005	1300.5	619.8	1512.1	1288.1
2006	1748.4	1257.8	1688.3	1723.5
2007	1298.4	427.9	1306.7	1414.3
2008	1577.9	603.9	1444.8	1450.4
MEAN	1357.8	811.5	1429.9	1353.0
% BIAS	0.4	-40.0	5.7	

Table 2: Total seasonal rainfall (June – September)

Date	3B42RT	3B42V6	3B42V7	Rain Gauge
2003	660.8	780.1	1108.4	911.8
2004	810.0	662.1	1040.5	853.7
2005	955.4	390.7	1130.1	935.7
2006	1117.7	706.7	1194.1	1255.0
2007	767.7	205.1	927.9	1064.3
2008	1062.0	416.7	1022.8	1037.1
MEAN	895.6	526.9	1070.6	1009.6
% BIAS	-11.3	-47.8	6.04	

Table 3: Percentage of seasonal rainfall

Date	3B42RT	3B42V6	3B42V7	Rain Gauge
2003	75.6	84.0	88.0	86.5
2004	60.1	64.2	76.1	71.9
2005	73.5	63.0	74.7	72.6
2006	63.9	56.2	70.7	72.8
2007	59.1	47.9	71.0	75.2
2008	67.3	69.0	70.8	71.5

Table 4: Mean Monthly rainfall for the period of 2003-2008

Date	3B42RT	3B42V6	3B42V7	Rain Gauge
Jan	13.59	13.40	5.90	11.68
Feb	31.90	18.49	13.06	13.49
Mar	54.69	39.40	43.92	36.28
Apr	106.39	41.85	58.27	48.37
May	137.56	67.91	104.07	86.76
Jun	164.11	81.11	231.08	187.63
Jul	292.37	207.09	345.33	349.72
Aug	264.57	173.59	286.15	275.51
Sep	154.28	124.86	199.12	191.24
Oct	85.99	58.01	84.14	95.88
Nov	29.05	27.21	29.61	26.71
Dec	14.29	16.99	12.86	20.29

Table 5: Pearson correlation coefficient (R) of daily rainfall

R	3B42RT	3B42V6	3B42V7	Rain Gauge
3B42RT	1	0.65	0.69	0.45
3B42V6	0.65	1	0.73	0.4
3B42V7	0.69	0.73	1	0.51
Rain Gauge	0.45	0.4	0.41	1

Table 6: Pearson correlation coefficient (R) of monthly rainfall

R	3B42RT	3B42V6	3B42V7	Rain Gauge
3B42RT	1.00	0.70	0.87	0.86
3B42V6	0.70	1.00	0.80	0.76
3B42V7	0.87	0.80	1.00	0.93
Rain Gauge	0.87	0.77	0.93	1.00

Table 7: Sample daily rainfall RF [mm], temperature T [^{o}C], observed streamflow Q [mm/d], and evaporation Evap [mm] data used in the calibration of HBV - light model.

Birr watershed

Date	RF[mm]	T [^{o}C]	Q [mm/day]	Evap [mm]
20030101	0	19.75	0.243	1.19
20030102	0	19.85	0.243	0
20030103	0	20.1	0.242	1.34
20030104	0	19.6	0.233	1.52
20030105	0	18.75	0.231	1.43
20030106	0	20.75	0.23	1.43
20030107	0	22.25	0.221	1.2
20030108	0	22.5	0.218	1.47
20030109	0	22.5	0.21	1.64
20030110	0	22.35	0.218	0
20030111	0	22.35	0.219	1.47
20030112	0	21.95	0.218	1.43
20030113	0	19.25	0.21	1.56
20030114	0	20	0.213	1.58
20030115	0	20.6	0.19	1.65
20030116	0	20.7	0.184	1.65
20030117	0	20.25	0.175	1.56
20030118	0	20.9	0.166	0
20030119	0	20.75	0.164	1.34
20030120	0	21.85	0.157	1.32
20030121	0	21.25	0.155	1.45
20030122	0	21.6	0.154	1.34
20030123	0	21.25	0.147	1.34
20030124	0	22.6	0.15	1.7
20030125	0	21.65	0.169	1.63
20030126	0	21.75	0.158	0
20030127	0	22.5	0.154	1.7
20030128	0	22.25	0.147	1.61
20030129	0.391	22.5	0.145	1.39
20030130	0	24	0.137	1.35
20030131	0	22.5	0.132	1.96

Table 8: Sample of daily streamflow simulation based various rainfall inputs

Date	Observed	Rain gauge	3B42RT	3B42V7	3B42V6
01-Jan-04	0.208	0.039	0.02	0.019	0.003
02-Jan-04	0.206	0.035	0.019	0.017	0.003
03-Jan-04	0.198	0.032	0.018	0.016	0.004
04-Jan-04	0.196	0.029	0.017	0.014	0.006
05-Jan-04	0.195	0.026	0.015	0.013	0.006
06-Jan-04	0.187	0.024	0.014	0.012	0.005
07-Jan-04	0.184	0.021	0.018	0.011	0.005
08-Jan-04	0.177	0.019	0.017	0.01	0.007
09-Jan-04	0.175	0.018	0.016	0.009	0.006
10-Jan-04	0.178	0.016	0.015	0.008	0.006
11-Jan-04	0.195	0.014	0.013	0.008	0.005
12-Jan-04	0.205	0.013	0.015	0.01	0.006
13-Jan-04	0.198	0.012	0.029	0.04	0.046
14-Jan-04	0.196	0.011	0.04	0.037	0.042
15-Jan-04	0.196	0.01	0.039	0.034	0.038
16-Jan-04	0.195	0.009	0.037	0.03	0.034
17-Jan-04	0.187	0.008	0.034	0.027	0.031
18-Jan-04	0.184	0.007	0.031	0.025	0.028
19-Jan-04	0.177	0.006	0.028	0.023	0.025
20-Jan-04	0.175	0.006	0.025	0.02	0.023
21-Jan-04	0.174	0.005	0.023	0.019	0.021
22-Jan-04	0.168	0.005	0.021	0.017	0.019
23-Jan-04	0.174	0.004	0.019	0.015	0.017
24-Jan-04	0.175	0.004	0.019	0.014	0.015
25-Jan-04	0.175	0.004	0.018	0.013	0.014
26-Jan-04	0.175	0.003	0.017	0.011	0.013
27-Jan-04	0.173	0.003	0.024	0.013	0.036
28-Jan-04	0.158	0.003	0.029	0.013	0.04
29-Jan-04	0.155	0.002	0.034	0.012	0.036
30-Jan-04	0.155	0.002	0.042	0.012	0.034
31-Jan-04	0.154	0.002	0.045	0.013	0.031

Table 9:Pearson correlation coefficient (R) of daily streamflow simulation

R	Observed	Rain gauge	3B42RT	3B42V7	3B42V6
Observed	1.00	0.84	0.77	0.77	0.58
Rain gauge	0.84	1.00	0.86	0.84	0.69
3B42RT	0.77	0.86	1.00	0.89	0.72
3B42V7	0.77	0.84	0.89	1.00	0.76
3B42V6	0.58	0.69	0.72	0.76	1.00

Table 10: Pearson correlation coefficient (R) of monthly streamflow simulation

R	Observed	Rain gauge	3B42RT	3B42V7	3B42V6
Observed	1.00	0.95	0.92	0.90	0.67
Rain gauge	0.95	1.00	0.96	0.94	0.75
3B42RT	0.92	0.96	1.00	0.94	0.76
3B42V7	0.90	0.94	0.94	1.00	0.78
3B42V6	0.67	0.75	0.76	0.78	1.00

Table 11: Performance statistics of model simulation based various rainfall inputs

	NSE	r^2	% BIAS
Rain gauge	0.71	0.71	-2.56
3B42RT	0.60	0.60	-0.15
3B42V7	0.57	0.59	1.31
3B42V6	0.18	0.34	-55.63

Table 12: Performance statistics of model calibrated using EXISTING rain gauge data

	NEW	EXISTING	OSESERVED
Total	432.72	403.8	404.7
% BIAS	6.93	-0.22	
NSE	0.32	0.28	
r^2	0.36	0.28	

Table 13: Performance statistics of model calibrated using NEW rain gauge data

	NEW	EXISTING	OSESERVED
Total	404.6	374.4	404.7
% BIAS	-0.03	-7.49	
NSE	0.32	0.14	
r^2	0.38	0.20	

Table 13: Sample of Exceedence probability (EP) of observed and simulated daily streamflow

Observed	EP of observed	Qsim_ Rain gauge	EP of Rain gauge	Qsim_ 3B42RT	EP of 3B42RT	Qsim_ 3B42V7	EP of 3B42V7	Qsim_ 3B42V6	EP of 3B42V6
14.25	0.05	11.22	0.05	11.80	0.05	13.91	0.05	8.09	0.05
13.98	0.11	9.62	0.11	10.13	0.11	13.31	0.11	6.40	0.11
13.50	0.16	9.40	0.16	10.06	0.16	13.25	0.16	5.32	0.16
13.27	0.22	8.80	0.22	9.93	0.22	11.63	0.22	5.08	0.22
13.21	0.27	8.44	0.27	9.29	0.27	11.19	0.27	5.03	0.27
12.54	0.33	8.26	0.33	9.06	0.33	10.99	0.33	4.64	0.33
12.51	0.38	8.25	0.38	8.99	0.38	10.14	0.38	4.47	0.38
11.45	0.44	8.21	0.44	8.94	0.44	9.77	0.44	4.44	0.44
11.45	0.49	8.19	0.49	8.79	0.49	9.70	0.49	4.15	0.49
11.35	0.55	8.10	0.55	8.59	0.55	9.41	0.55	4.05	0.55
11.25	0.60	7.93	0.60	8.44	0.60	9.00	0.60	4.01	0.60
11.25	0.66	7.57	0.66	8.35	0.66	8.95	0.66	3.96	0.66
11.25	0.71	7.57	0.71	8.33	0.71	8.85	0.71	3.95	0.71
11.24	0.77	7.46	0.77	8.23	0.77	8.73	0.77	3.95	0.77
11.21	0.82	7.27	0.82	8.19	0.82	8.37	0.82	3.93	0.82
11.12	0.88	7.07	0.88	8.08	0.88	7.68	0.88	3.86	0.88
10.97	0.93	7.07	0.93	7.41	0.93	7.64	0.93	3.81	0.93
10.38	0.98	7.04	0.98	7.35	0.98	7.39	0.98	3.81	0.98
10.26	1.04	6.84	1.04	7.34	1.04	7.38	1.04	3.76	1.04
10.25	1.09	6.84	1.09	7.30	1.09	7.35	1.09	3.68	1.09
10.25	1.15	6.78	1.15	7.27	1.15	7.13	1.15	3.55	1.15
10.25	1.20	6.68	1.20	7.26	1.20	7.00	1.20	3.54	1.20
10.15	1.26	6.68	1.26	7.04	1.26	6.83	1.26	3.53	1.26
10.04	1.31	6.61	1.31	7.00	1.31	6.79	1.31	3.49	1.31
9.81	1.37	6.47	1.37	6.94	1.37	6.73	1.37	3.46	1.37
9.59	1.42	6.46	1.42	6.94	1.42	6.52	1.42	3.46	1.42
9.25	1.48	6.36	1.48	6.92	1.48	6.42	1.48	3.46	1.48
8.54	1.53	6.35	1.53	6.83	1.53	6.31	1.53	3.45	1.53
8.51	1.59	6.33	1.59	6.82	1.59	6.16	1.59	3.43	1.59
8.37	1.64	6.33	1.64	6.82	1.64	6.06	1.64	3.39	1.64
8.25	1.70	6.24	1.70	6.79	1.70	6.01	1.70	3.39	1.70
8.12	1.75	6.20	1.75	6.71	1.75	6.01	1.75	3.38	1.75
8.02	1.81	6.19	1.81	6.63	1.81	5.98	1.81	3.34	1.81
8.02	1.86	6.10	1.86	6.54	1.86	5.91	1.86	3.28	1.86
8.00	1.91	6.04	1.91	6.47	1.91	5.76	1.91	3.25	1.91

Appendix II List of Figures

1. Comparison of average rainfall magnitude from various rainfall products. Figure 1 shows the total average rainfall for satellite and rain gauges for the period of 08 July to 30 September 30 2012.

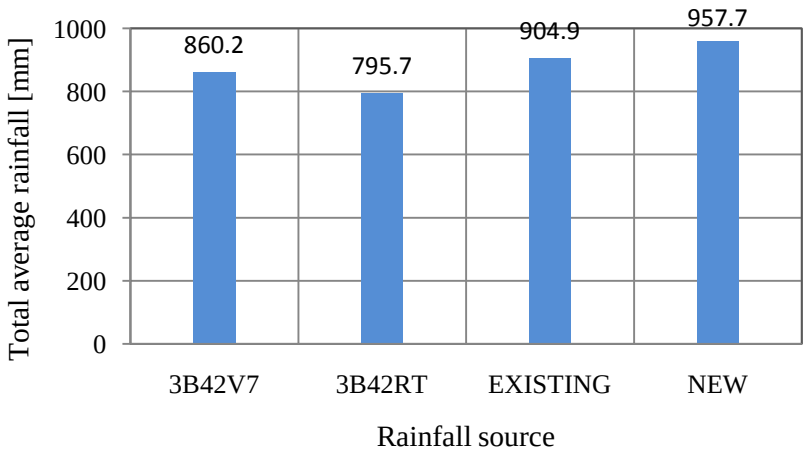

Fig.1 Total average rainfall comparison for the rainy season of 08 July – 30 September 2012, from various rainfall sources.

2. Model calibration rainfall input from newly deployed and existing rain gauges

We tried to calibrate HBV – light model using rainfall inputs from two different sources: (i) three existing meteorological rain gauge station and (ii) eleven newly installed Tipping Bucket rain gauges for the rain season from 08 July to 30 September 2012. The main purpose of this comparison was to check the performance of model simulation when subjected to sparse and relatively dense rain gauge networks. The comparison of observed and model simulation results using rainfall inputs form new rain gauge (NEW) and existing rain gauge (EXISTING) was analyzed for two cases:

Case – I: model calibration using rainfall inputs from existing rain gauges:

We compared the result of model simulation based new rain gauges with observed daily stream flow.

Case – II: Calibration using rainfall inputs from new rain gauges:

We compared the result of model simulation based on existing rain gauges with observed daily streamflow.

Case – I: model calibration using rainfall inputs from existing rain gauges

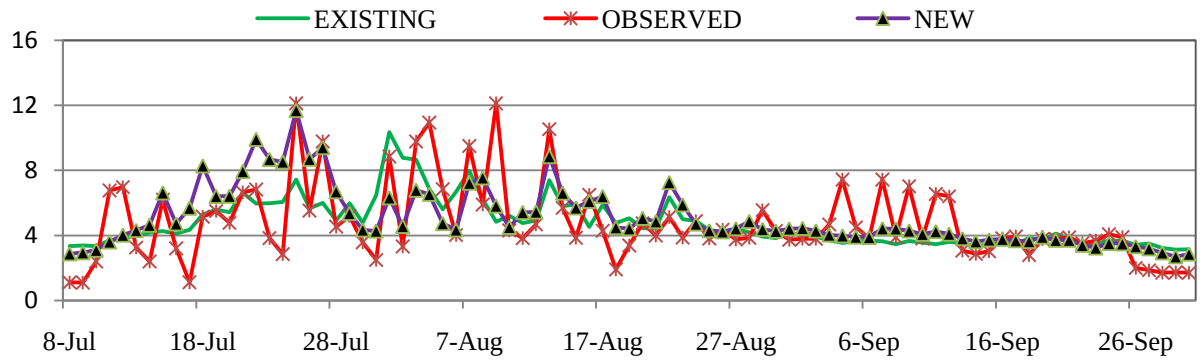

Fig. 2 Comparison result of observed and simulated daily streamflow when model parameter calibrated using rainfall from existing rain gauge over Birr watershed.

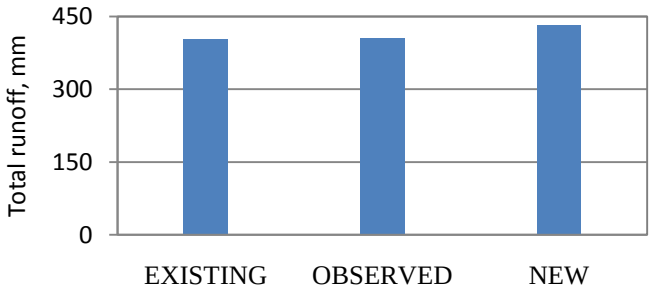

Fig. 3 Total observed and simulated runoff comparison when model parameter calibrated using rainfall from existing rain gauge over Birr watershed.

Case – II: Calibration using rainfall inputs from new rain gauges

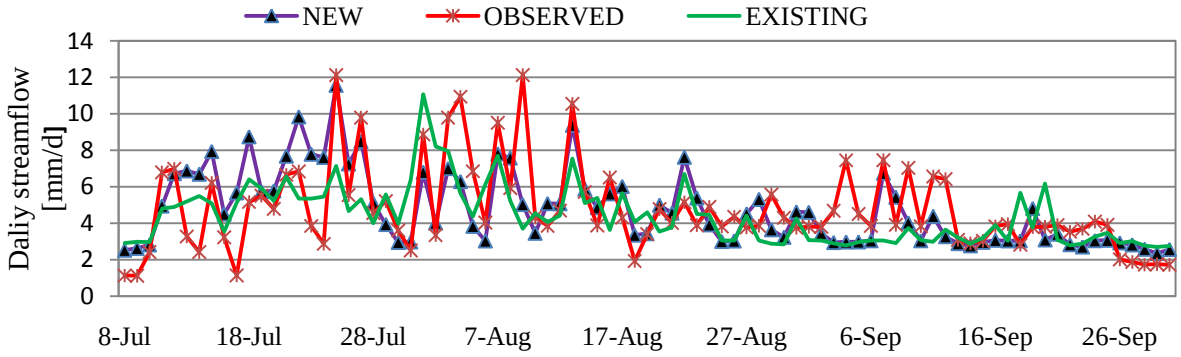

Fig. 4 Comparison result of observed and simulated daily streamflow when model parameter calibrated using rainfall from new rain gauge over Birr watershed.

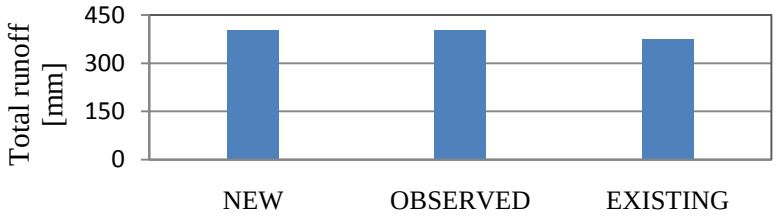

Fig. 5 Total observed and simulated runoff comparison when model parameter calibrated using rainfall from new rain gauge over Birr watershed.

3. Comparison result of simulated monthly streamflow based various rainfall inputs with observed daily streamflow over the watershed.

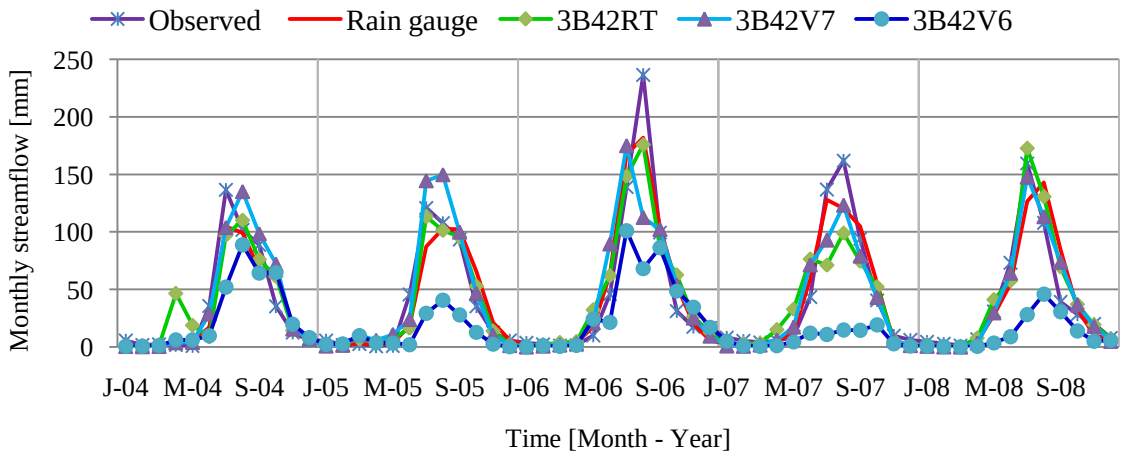

Fig. 6 The comparison of monthly observed and monthly simulated based on satellite and rain gauge rainfall inputs using model calibrated with existing rain gauge rainfall data.

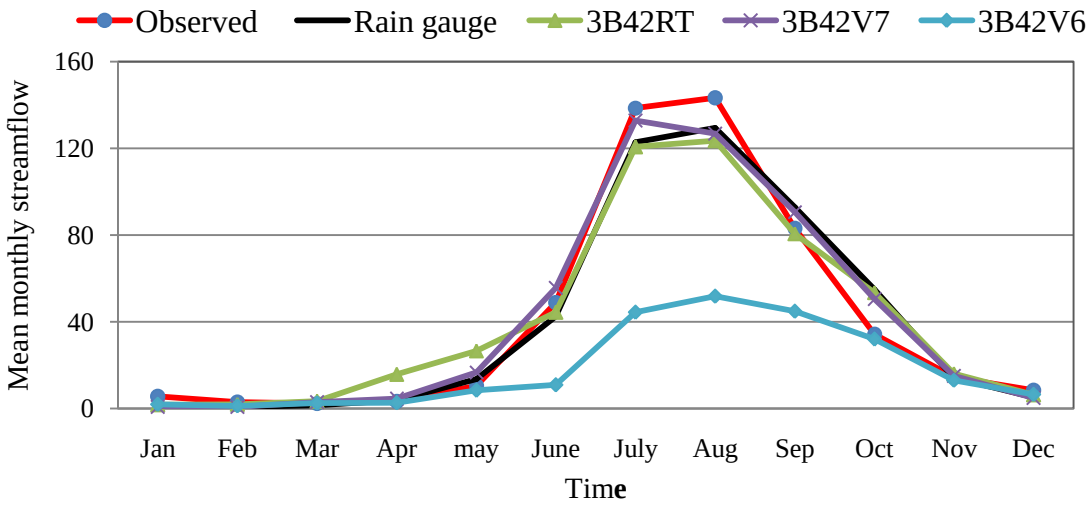

Fig. 7 Comparison of observed and model simulated mean monthly streamflow for various rainfall inputs.